

# Exploring the Growth-Index ( $\gamma$ ) Tension with $\Lambda_s$ CDM

Luis A. Escamilla,<sup>1,\*</sup> Özgür Akarsu,<sup>2,†</sup> Eleonora Di Valentino,<sup>1,‡</sup> Emre Özülker,<sup>1,§</sup> and J. Alberto Vazquez<sup>3,¶</sup>

<sup>1</sup>*School of Mathematical and Physical Sciences, University of Sheffield,  
Hounsfield Road, Sheffield S3 7RH, United Kingdom*

<sup>2</sup>*Department of Physics, Istanbul Technical University, Maslak 34469 Istanbul, Turkey*

<sup>3</sup>*Instituto de Ciencias Físicas, Universidad Nacional Autónoma de México, Cuernavaca, Morelos, 62210, México*

Recent observational analyses have revealed a significant tension in the growth index  $\gamma$ , which characterizes the growth rate of cosmic structures. Specifically, when treating  $\gamma$  as a free parameter within  $\Lambda$ CDM framework, a combination of Planck and  $f\sigma_8$  data yields  $\gamma \approx 0.64$ , in  $\sim 4\sigma$  tension with the theoretically expected value  $\gamma \approx 0.55$  (assuming general relativity). This discrepancy, closely related to the  $S_8$  tension, poses a new challenge to the standard cosmological model by suggesting that it predicts an excessive growth of structure. In this work, we demonstrate that the  $\Lambda_s$ CDM framework—featuring a rapid sign-switching cosmological constant (mirror AdS-to-dS transition) in the late universe at redshift  $z_\dagger \sim 2$ —can simultaneously alleviate the  $\gamma$ ,  $H_0$ , and  $S_8$  tensions. We also examined a scenario with fixed  $z_\dagger = 1.7$ , previously identified as a sweet spot for alleviating multiple major cosmological tensions—including those in  $H_0$ ,  $M_B$ , and  $S_8$ —finding that it completely eliminates both the  $\gamma$  and  $H_0$  tensions, although it is statistically disfavored by our dataset combinations. Our findings suggest that  $\Lambda_s$ CDM is a promising model, providing a potential unified resolution to multiple major cosmological tensions.

## I. INTRODUCTION

It is well established that, despite its status as the prevailing cosmological paradigm, the standard  $\Lambda$ CDM model faces several important observational challenges and inconsistencies, which appear to be intensifying as cosmological data become increasingly precise. Some of these issues relate to fundamental gaps in our understanding of the dark sector, comprising dark matter (DM) and dark energy (DE). Others are statistical in nature, but equally significant, most notably the well-documented  $H_0$  (Hubble constant) tension [1–15], and the  $S_8$  (weighted amplitude of matter fluctuations) tension [15–30]. In addition to these established discrepancies, recent analyses have identified a new tension associated with the growth rate of cosmic structures, which deviates significantly from expectations within the standard model framework [31, 32].

The linear growth rate of matter density perturbations, defined as  $f(a) \equiv \frac{d \ln \delta(a)}{d \ln a}$ , where  $\delta(a)$  is the matter density contrast and  $a$  is the scale factor, characterizes the dynamical evolution of cosmic structures under gravitational instability. Within the framework of general relativity (GR), this quantity can be reliably approximated by the power-law ansatz  $f(a) \approx \Omega_m(a)^\gamma$  [33, 34], where  $\Omega_m(a) = \frac{\Omega_{m0} H_0^2}{H^2}$  is the normalized matter density parameter, and  $\gamma$  is the growth index, a parameter encapsulating the influence of cosmic expansion on structure formation. In the standard  $\Lambda$ CDM cosmology, assuming a spatially flat universe and GR as the underlying theory

of gravity, the growth index is predicted to be  $\gamma \approx 0.55$  with high accuracy. Precise observational constraints on  $f(a)$ , particularly at low redshifts, provide a powerful probe of the nature of dark energy, the properties of dark matter, and potential deviations from GR on cosmological scales [35]. Any statistically significant departure from  $\gamma \approx 0.55$  may signal the presence of new physics, such as modifications to gravity or interactions beyond the Standard Model (SM) of particle physics.

In Ref. [31], it was demonstrated that when the growth index  $\gamma$  is treated as a free parameter within  $\Lambda$ CDM and inferred from large-scale structure and Planck Cosmic Microwave Background (CMB) data, a tension exceeding  $4\sigma$  arises relative to the theoretically expected value of  $\gamma \approx 0.55$ . This discrepancy might be linked to the well-known  $A_{\text{lens}}$  problem [31, 32, 36–39]. Given the worrisome, longstanding tensions and newly emerging ones, such as the  $\gamma$  tension,<sup>1</sup> within  $\Lambda$ CDM, it is natural to explore alternative frameworks that may provide a viable resolution. In this context, the  $\Lambda_s$ CDM model emerged as a promising candidate.

The so-called  $\Lambda_s$ CDM framework [40–43] stands out as a promising and economical extension of  $\Lambda$ CDM, capable of addressing major cosmological tensions—including those in  $H_0$ ,  $M_B$  (Type Ia Supernovae absolute magnitude), and  $S_8$ —as well as the Baryon Acoustic Oscillations (BAO) Ly- $\alpha$  anomaly, while simultaneously yielding an age of the Universe consistent with estimates from the oldest globular clusters and, when treated as free parameters, without spoiling a total neutrino mass and an effective number of species in agreement with the SM of particle physics [40–46]. Because of the latter feature studied in [46], we can

\* l.a.escamilla@sheffield.ac.uk

† akarsuo@itu.edu.tr

‡ e.divalentino@sheffield.ac.uk

§ e.ozulker@sheffield.ac.uk

¶ javazquez@icf.unam.mx

<sup>1</sup> It is important to note that many of the tensions are not completely independent, e.g., the  $H_0$  and  $M_B$  tensions noted below. Similarly, the  $\gamma$  tension is closely related to the  $S_8$  tension.

speculate that the  $\Lambda_s$ CDM framework may circumvent the recently proposed anomaly wherein cosmological data (e.g., DESI BAO), analyzed within the standard  $\Lambda$ CDM framework, appear to favor  $m_\nu < 0$  [47–52], as it happens for other models of DE [53]. Motivated by this success of  $\Lambda_s$ CDM, we explore  $\Lambda_s$ CDM’s potential to resolve the recently identified  $\gamma$  tension [31] by examining whether it naturally explains the observed suppression of cosmic structure growth, while still remaining consistent with the theoretically expected value,  $\gamma \approx 0.55$  (assuming GR). We first briefly review the  $\Lambda_s$ CDM framework and provide insight into why it has the potential to address the  $\gamma$  tension, along with the  $H_0$  and  $S_8$  tensions. Then, following the approach of Ref. [31], we extend both the  $\Lambda_s$ CDM and  $\Lambda$ CDM models by treating  $\gamma$  as a free parameter, constraining them using Planck CMB and  $f\sigma_8$  data, and subsequently incorporating additional cosmological datasets such as Type Ia Supernovae (SN Ia) and BAO data. This allows us to assess the capability of  $\Lambda_s$ CDM in addressing the  $\gamma$  tension, while simultaneously evaluating the status of the  $H_0$  and  $S_8$  tensions. Our analysis yields promising results—though with some compromise when BAO data is included—and reveals a clear correlation in the alleviation of the  $\gamma$  and  $H_0$  tensions, reinforcing the possibility of a unified resolution to the major cosmological tensions within the  $\Lambda_s$ CDM framework.

## II. INSIGHTS INTO $\Lambda_s$ CDM AND JOINTLY ADDRESSING THE $\gamma$ , $H_0$ , AND $S_8$ TENSIONS

The  $\Lambda_s$ CDM framework, originally conjectured phenomenologically in Ref. [40] based on findings from the graduated dark energy (gDE) model, posits that around redshift  $z_\dagger \sim 2$ , the Universe underwent a period of rapid *mirror* AdS-to-dS (anti-de Sitter-to-de Sitter) transition in vacuum energy—namely, a rapid sign-switching cosmological constant (CC),  $\Lambda_s$ , from negative to positive while preserving its overall magnitude (“mirror” reflects this invariance)—or a similar phenomenon, all while leaving other standard cosmological components, such as baryons, CDM, pre-recombination physics, and the inflation paradigm, unaltered. Such transitions can typically be described using sigmoid-like functions; for example,  $\Lambda_s(z) = \Lambda_{s0} \tanh[\nu(z_\dagger - z)] / \tanh[\nu z_\dagger]$ , where  $\nu > 1$  controls the sharpness of the transition,  $\Lambda_{s0} > 0$  is the present-day value, and  $z_\dagger$  denotes the transition redshift. For a sufficiently rapid transition, e.g.,  $\nu \gtrsim 10$  at  $z_\dagger \sim 2$ , this function approximates a smooth step-like behavior with  $\Lambda_s \approx \Lambda_{s0}$  for  $z \lesssim 2$  and  $\Lambda_s \approx -\Lambda_{s0}$  for  $z \gtrsim 2$ , effectively characterized by a single parameter,  $z_\dagger$  [45]. In the limiting case  $\nu \rightarrow \infty$ , the transition becomes instantaneous:

$$\Lambda_s(z) \rightarrow \Lambda_{s0} \operatorname{sgn}(z_\dagger - z), \quad (1)$$

which defines the *abrupt*  $\Lambda_s$ CDM model [41–43]—an idealized representation of a rapid mirror AdS-to-dS transition extending  $\Lambda$ CDM by a single additional parameter,  $z_\dagger$ . This is the simplest phenomenological realization

of the  $\Lambda_s$ CDM framework, which has been extensively studied [41–43, 45, 46] under the assumption that gravity is governed by GR. Its *abrupt* transition at  $z = z_\dagger$  introduces a discontinuity, resulting in a type II (sudden) singularity [54] at  $z = z_\dagger$ . Nonetheless, Ref. [55] has demonstrated that this singularity itself has a negligible impact on bound cosmic structures and their formation and evolution, and it disappears when the transition is smoothed out. From a mathematical/physical standpoint, this framework remains identical to  $\Lambda$ CDM at redshifts  $z < z_\dagger$ , where it features a dS-like CC after the transition, but introduces a minimal modification by incorporating an AdS-like CC for all redshifts prior to the transition,  $z > z_\dagger$ . However, from a phenomenological perspective—i.e., considering the expansion dynamics and observational signatures—the impact of this modification is effectively limited to redshifts  $z \lesssim z_\dagger \sim 2$ . Specifically, for  $z < z_\dagger$ ,  $\Lambda_s$ CDM closely replicates the expansion history  $H(z)$  of  $\Lambda$ CDM, albeit with systematically higher values; it introduces a noticeable deformation of  $H(z)$  around the transition redshift  $z \sim z_\dagger$  and becomes virtually indistinguishable from  $\Lambda$ CDM at higher redshifts ( $z \gtrsim 3$ ). Consequently, from a phenomenological standpoint,  $\Lambda_s$ CDM functions as a post-recombination, late-time modification of  $\Lambda$ CDM. For notable explicit physical realizations of this scenario—both in its abrupt and smooth formulations—see, for example, Refs. [44, 45, 56–62], which explore its implementation within various well-founded theoretical frameworks.<sup>2</sup>

In this scenario, since the pre-recombination Universe remains unaltered, as in  $\Lambda$ CDM, the comoving sound horizon at last scattering,  $r_*$ , remains effectively unchanged. The Planck CMB spectra provide precise measurements of the angular scale of the sound horizon,  $\theta_* = r_*/D_M(z_*)$ , and the present-day physical matter density,  $\Omega_{m0}h^2$  (here,  $h = H_0/100 \text{ km s}^{-1} \text{ Mpc}^{-1}$  is the dimensionless reduced

<sup>2</sup> For further theoretical and observational studies—including model-agnostic reconstructions—investigating DE (whether as a physical source or an effective source arising from, e.g., modified gravity) that features negative energy densities at high redshifts ( $z \gtrsim 1.5$ –2), often consistent with a negative (AdS-like) CC and aimed at addressing cosmological tensions, we refer the reader, without claiming to be exhaustive, to Refs. [56–129]. Phantom DE models, traditionally assumed to yield only positive energy densities, are well known for alleviating the  $H_0$  tension. Among these, the so-called *phantom crossing model* [83] (DMS20 [105]) stands out; a recent analysis [105] reaffirming its success also revealed that its ability to assume negative densities for  $z \gtrsim 2$ —mimicking an AdS-like CC at higher redshifts—plays a central role in its effectiveness. Interacting DE (IDE) models [126, 130–145] provide an alternative approach to alleviating the  $H_0$  tension, yet model-independent reconstructions of interaction kernels [104] suggest their energy densities tend to become negative at  $z \gtrsim 2$ . Recent DESI BAO data—analyzed using the CPL parameterization—provided more than  $3\sigma$  evidence for dynamical DE [146], while non-parametric reconstructions of the same data further indicate that this dynamical behavior may involve vanishing or negative DE densities for  $z \gtrsim 1.5$ –2 [114, 122], a trend similarly observed in pre-DESI BAO data from SDSS [120, 122].

Hubble constant), inferred from the peak structure and damping tail. Consequently, both the comoving angular diameter distance to last scattering,  $D_M(z_*)$ , and  $\Omega_{m0}h^2$  must remain consistent with their Planck- $\Lambda$ CDM inferred values. Any suppression of  $H(z)$  when  $z > z_\dagger$ , caused by the AdS-like CC, must therefore be compensated by an enhancement of  $H(z)$  when  $z < z_\dagger$  during the dS-like CC regime to preserve consistency with Planck- $\Lambda$ CDM inferred  $D_M(z_*)$ . This mechanism naturally increases  $H_0$  while lowering  $\Omega_{m0}$  relative to Planck- $\Lambda$ CDM. A later transition (i.e., a smaller  $z_\dagger$ ) prolongs the suppression of  $H(z)$  and deepens it at later times, amplifying both effects, provided that the transition occurs before the AdS-like CC dominates and halts expansion. Additionally, the suppression of  $H(z)$  for  $z > z_\dagger$  reduces cosmic friction, thereby enhancing structure formation in this regime, which could potentially lead to an increase in  $\sigma_8$  (amplitude of mass fluctuations on scales of  $8 h^{-1}$  Mpc). However, the reduced present-day matter density can still lower  $S_8 = \sigma_8 \sqrt{\Omega_{m0}/0.3}$  and thereby alleviate the  $S_8$  tension. Similarly, since the linear growth rate of matter perturbations  $f$  is related to the growth index  $\gamma$  through  $f(a) \approx \Omega_m(a)^\gamma$ , with  $\gamma \approx 0.55$  in GR, a late-time suppression in  $f$  can be achieved through reduced values of  $\Omega_m(a)$  relative to  $\Lambda$ CDM at  $z < z_\dagger$  while still maintaining  $\gamma \sim 0.55$ —thus making the same mechanism responsible for alleviating the  $S_8$  tension a compelling candidate for addressing the  $\gamma$  tension as well.

A theoretical study of the abrupt  $\Lambda_s$ CDM model in Ref. [147], within GR, reveals a two-phase evolution of linear matter density perturbations. Before the transition, during the AdS-like CC regime, the negative cosmological constant reduces cosmic friction, enhancing the growth rate of matter perturbations relative to  $\Lambda$ CDM, with the effect peaking just before the transition. After the transition, the model closely follows  $\Lambda$ CDM but with a larger dS-like CC, leading to higher expansion rates  $H(z)$  and stronger cosmic friction, which more effectively suppresses structure growth at late times. Specifically, before the transition, the growth index  $\gamma$  remains below the Einstein–de Sitter value ( $\gamma \approx 6/11$ ) [33] and thus lower than in  $\Lambda$ CDM. As the transition occurs,  $\gamma$  rises sharply and then evolves gradually, closely tracking the  $\Lambda$ CDM prediction while staying slightly elevated post-transition. Nevertheless,  $\gamma$  remains near 0.55 throughout, consistent with standard  $\Lambda$ CDM expectations; see Figure 11 in Ref. [147]. Using  $\gamma = 0.55$  and the Planck- $\Lambda$ CDM prediction of  $\Omega_{m0} \simeq 0.32$ , the corresponding present-day growth rate is  $f_0 \simeq 0.53$ . However, Nguyen et al. [31], extending  $\Lambda$ CDM by treating  $\gamma$  as a free parameter constrained by observational data, report  $\gamma \simeq 0.63$ , leading to a suppressed growth rate of  $f_0 \simeq 0.48$ , indicating a deviation from  $\Lambda$ CDM and a suppression of structure growth at low redshifts. Observational analyses show that  $\Lambda_s$ CDM generally predicts lower  $\Omega_{m0}$  than  $\Lambda$ CDM [41–43, 45]; specifically, Planck- $\Lambda_s$ CDM yields  $\Omega_{m0} \simeq 0.28$ , corresponding to  $f_0 \simeq 0.49$ , closely matching Ref. [31]. Moreover, it was shown that for  $z_\dagger \approx 1.7$ ,  $\Lambda_s$ CDM re-

solves both the  $H_0$  and  $S_8$  tensions, bringing them below  $\sim 1\sigma$  [43] by predicting  $\Omega_{m0} = 0.27$ , which in turn gives  $f_0 = 0.48$ , in precise agreement with the inferred  $\gamma$  in [31].

This trend parallels the way  $\Lambda_s$ CDM alleviates the  $S_8$  tension, primarily through subtle modifications in the CMB constraints, effectively reducing the discrepancy from  $3.1\sigma$  in  $\Lambda$ CDM to approximately  $1.7\sigma$ . Notably, since  $\Lambda_s$ CDM is identical to  $\Lambda$ CDM after the transition (for  $z \lesssim z_\dagger \sim 2$ ), its KiDS-1000-alone constraint closely matches that of  $\Lambda$ CDM, yielding  $S_8 = 0.746^{+0.026}_{-0.021}$  compared to  $S_8 = 0.749^{+0.027}_{-0.020}$  in  $\Lambda$ CDM. However, in the Planck-alone analysis,  $\Lambda_s$ CDM predicts only a slightly larger  $\sigma_8$  than  $\Lambda$ CDM. Consequently, by significantly reducing  $\Omega_{m0}$ —and given the positive correlation between  $S_8$  and  $\Omega_{m0}$  (which itself depends on the transition redshift  $z_\dagger$ )—the model naturally shifts  $S_8$  to lower values, improving agreement with its KiDS-1000-alone constraints. Specifically, the Planck-alone analysis yields  $S_8 = 0.801^{+0.026}_{-0.016}$  in  $\Lambda_s$ CDM, leading to only a  $1\sigma$  tension with KiDS-1000, whereas Planck- $\Lambda$ CDM gives  $S_8 = 0.832 \pm 0.013$ , resulting in a  $3.1\sigma$  discrepancy. Just as the interplay between  $\Omega_{m0}$  and  $S_8$  allows  $\Lambda_s$ CDM to alleviate the  $S_8$  tension, its inherent tendency to predict lower  $\Omega_{m0}$  values relative to  $\Lambda$ CDM in observational analyses provides a potential explanation for the suppression of structure growth reported in [31]. Rather than requiring an anomalously high  $\gamma \approx 0.63$ , as inferred when  $\gamma$  is treated as a free parameter in  $\Lambda$ CDM [31],  $\Lambda_s$ CDM has the potential to achieve a similar suppression by reducing  $\Omega_m(a)$ , and correspondingly  $\Omega_{m0}$  as well, in the late universe while maintaining  $\gamma \approx 0.55$ , as expected in GR.

Consequently, the  $\Lambda_s$ CDM framework presents a compelling possibility for a unified explanation of the major cosmological tensions—namely, the  $H_0$ ,  $S_8$ , and the recently identified  $\gamma$  tensions—through a single underlying physical mechanism. In the following, we examine this potential by considering the *abrupt*  $\Lambda_s$ CDM scenario [41–43] as a proxy for rapid transitions, under the assumption that gravity is governed by GR.

### III. METHODOLOGY AND DATA

In this work, we focus on two models:  $\gamma\Lambda$ CDM and  $\gamma\Lambda_s$ CDM, which extend  $\Lambda$ CDM and abrupt  $\Lambda_s$ CDM by treating  $\gamma$  as a free parameter, yielding seven and eight free parameters, respectively. Both models share seven parameters, six of which are standard in  $\Lambda$ CDM: the physical baryon density  $\Omega_b h^2$ , the physical cold dark matter density  $\Omega_c h^2$ , the optical depth  $\tau$ , the angular scale of the sound horizon at recombination  $\theta_s$ , the amplitude of primordial scalar perturbations  $\log(10^{10} A_s)$ , and the scalar spectral index  $n_s$ . The seventh shared parameter is the growth index  $\gamma$ , which governs the evolution of matter perturbations. The distinguishing feature of  $\gamma\Lambda_s$ CDM is an additional parameter,  $z_\dagger$ , which sets the redshift of the mirror AdS-to-dS transition. We consider the extension of the abrupt  $\Lambda_s$ CDM framework (1) for simplicity, serving



TABLE I. Ranges for the flat prior distributions imposed on cosmological parameters.

Parameter	Prior
$\Omega_b h^2$	[0.005, 0.1]
$\Omega_c h^2$	[0.005, 0.99]
$\tau$	[0.01, 0.8]
$100 \theta_s$	[0.5, 10]
$\log(10^{10} A_S)$	[1.61, 3.91]
$n_s$	[0.8, 1.2]
$\gamma$	[0.0, 2.0]
$z_{\dagger}$	[1.0, 3.0]

as a phenomenologically idealized proxy for a sufficiently rapid yet smooth mirror AdS-to-dS transition. The priors applied to each free parameter are summarized in Table I.

Given that the primary goal of this study is to compare the  $\gamma\Lambda$ CDM and  $\gamma\Lambda_s$ CDM models, particularly in terms of the inferred value of  $\gamma$  relative to the theoretical prediction  $\gamma \approx 0.55$ , a rigorous parameter inference analysis is essential. To accomplish this, we utilize **Cobaya** [148], a Markov Chain Monte Carlo (MCMC) sampler designed for cosmological models, in conjunction with **CAMB** [149], a Boltzmann solver. Specifically, we use a modified version called **CAMB GammaPrime Growth** [150] to account for the parameterization of the growth rate. To evaluate the convergence of our chains, we use the Gelman-Rubin parameter  $R - 1$  [151], adopting  $R - 1 < 0.01$  as the threshold value for convergence.

Alongside the  $\gamma\Lambda$ CDM and  $\gamma\Lambda_s$ CDM models, we also consider two special cases of  $\gamma\Lambda_s$ CDM in which the transition redshift is fixed at  $z_{\dagger} = 1.7$  and 2.16, effectively reducing the number of free parameters by one to match that of the  $\gamma\Lambda$ CDM model. The first choice is motivated by previous studies demonstrating that  $z_{\dagger} \approx 1.7$  effectively resolves multiple cosmological tensions, including those in  $H_0$ ,  $M_B$ , and  $S_8$  [41–43, 45, 46]. Thus, even though this specific transition redshift may not be directly favored by the datasets considered here, we find it insightful to explicitly examine this scenario due to its proven success in addressing major cosmological tensions. The second choice is instead suggested by the best-fit value  $z_{\dagger} \approx 2.16$  for the dataset combination PL18+ $f\sigma_8$ +PP&SH0ES which is the data set combination for which the  $\gamma\Lambda_s$ CDM model has the largest improvement in the fit to the data compared to  $\gamma\Lambda$ CDM.

To perform parameter inference and systematically compare the models under consideration, we utilize the following datasets:

- The *Planck* 2018 CMB temperature anisotropy and polarization power spectra, their cross-spectra, and the lensing reconstruction from the *Planck* 2018 legacy data release [152] (PR3). We refer to this dataset as **PL18**.
- Measurements of the  $f\sigma_8$  parameter combination

from redshift-space distortions (RSD), peculiar velocity, and cosmological distance measurements [153–163]. We refer to this dataset as  $f\sigma_8$ .

- Baryon Acoustic Oscillation (BAO) and Redshift-Space Distortion (RSD) measurements from the completed SDSS-IV eBOSS survey [163]. These include isotropic and anisotropic distance and expansion rate measurements at both low and high redshifts (including Lyman- $\alpha$  BAO data). We refer to this likelihood as **SDSS**.
- BAO distance measurements from the first year of observations with the Dark Energy Spectroscopic Instrument (DESI) [146]. We refer to this dataset as **DESI**. Given the risk of double counting, this dataset is not used in combination with **SDSS**.
- The catalog of 1701 light curves from 1550 distinct supernovae in the PantheonPlus SN Ia sample, covering a redshift range of  $0.01 < z < 2.26$  [164]. We refer to this dataset as **PP**.
- A Gaussian prior on the Hubble constant,  $H_0 = 73.04 \pm 1.04 \text{ km s}^{-1} \text{ Mpc}^{-1}$ , measured from SN Ia distances calibrated with Cepheids by the SH0ES team [165]. When using this prior, the term **SH0ES** is added in tandem with **PP**.

#### IV. RESULTS AND DISCUSSION

In this section, we present and interpret our parameter-inference results for the two main models— $\gamma\Lambda$ CDM and  $\gamma\Lambda_s$ CDM—as well as two special fixed- $z_{\dagger}$  cases of  $\gamma\Lambda_s$ CDM. We assess how each model addresses the growth-index tension by comparing the inferred  $\gamma$  to its theoretically expected value of  $\approx 0.55$ , while simultaneously examining the implications for the  $H_0$  and  $S_8$  tensions. We also pay special attention to the constraints on the present-day growth rate  $f_0 = \Omega_{m0}^\gamma$ , highlighting its role in distinguishing how  $\gamma\Lambda$ CDM and  $\gamma\Lambda_s$ CDM achieve late-time growth suppression. We present the constraints on the model parameters and relative  $\chi^2_{\min}$  values in Table II, along with the corresponding 1D and 2D posterior distributions arranged in triangle contour plots in Figs. 1–4. The corresponding tension significances for  $\gamma$  and  $H_0$  are summarized in Table III.

We observe that the  $\gamma\Lambda$ CDM extension continues to suffer from the  $\sim 5\sigma$   $H_0$  tension of standard  $\Lambda$ CDM, as seen in Tables II and III and Fig. 1. Across all dataset combinations—PL18, PL18+ $f\sigma_8$ , or even when including SN Ia/BAO—the  $H_0$  tension remains at the 3.8–4.7 $\sigma$  level. Simultaneously, the  $\gamma$  tension often exceeds 3 $\sigma$ , reaching its lowest value (1.8 $\sigma$ ) in the Planck-alone case, where  $\gamma = 0.662 \pm 0.063$ ; this lower significance is primarily due to the large uncertainties. The tension rises to 3.6 $\sigma$  for the PL18+ $f\sigma_8$  combination, yielding  $\gamma = 0.639 \pm 0.025$ —consistent with the findings of Ref. [31] for the same dataset combination—and peaks at 3.8 $\sigma$  for PL18+ $f\sigma_8$ +PP, where  $\gamma = 0.640 \pm 0.024$ . Furthermore, we observe that when the  $f\sigma_8$  likelihood is involved

TABLE II. Constraints on the growth index  $\gamma$  and selected cosmological parameters from extended combinations of datasets. The reported errors correspond to the 68% confidence level, except for  $z_{\dagger}$ , which is given at the 95% confidence level. The quantity  $\Delta\chi^2_{\min}$  indicates the difference in the fit of the data between the alternative model  $\gamma\Lambda_s\text{CDM}$  and  $\gamma\Lambda\text{CDM}$  for a given likelihood. If  $\Delta\chi^2_{\min} < 0$  ( $> 0$ ), then  $\gamma\Lambda_s\text{CDM}$  provides a better (worse) fit to the data.

Model	Data	$z_{\dagger}$	$\gamma$	$S_8$	$H_0$	$\Omega_{m0}$	$\Omega_{m0}^{\gamma}$	$\Delta\chi^2_{\min}$
$\gamma\Lambda_s\text{CDM}(z_{\dagger} \text{ free})$	PL18	$> 1.58$	$0.631 \pm 0.065$	$0.792 \pm 0.021$	$70.76^{+0.72}_{-2.1}$	$0.283^{+0.018}_{-0.001}$	$0.453^{+0.039}_{-0.045}$	1.33
	PL18+ $f\sigma_8$	$> 1.58$	$0.607 \pm 0.027$	$0.791 \pm 0.007$	$70.67^{+0.72}_{-2.0}$	$0.284^{+0.017}_{-0.008}$	$0.466 \pm 0.016$	-0.12
	PL18+ $f\sigma_8$ +PP	$> 2.12$	$0.621 \pm 0.024$	$0.807 \pm 0.011$	$69.12^{+0.53}_{-0.77}$	$0.298^{+0.008}_{-0.007}$	$0.472 \pm 0.015$	1.85
	PL18+ $f\sigma_8$ +PP&SH0ES	$> 1.79$	$0.610 \pm 0.025$	$0.794 \pm 0.011$	$70.42^{+0.74}_{-1.1}$	$0.286^{+0.009}_{-0.007}$	$0.466 \pm 0.016$	-4.66
	PL18+ $f\sigma_8$ +PP+SDSS	$> 2.29$	$0.624 \pm 0.024$	$0.813 \pm 0.007$	$68.66 \pm 0.44$	$0.303 \pm 0.005$	$0.475 \pm 0.014$	3.21
	PL18+ $f\sigma_8$ +PP+DESI	$> 2.40$	$0.623 \pm 0.024$	$0.801 \pm 0.007$	$68.98 \pm 0.41$	$0.295 \pm 0.005$	$0.461 \pm 0.014$	-1.18
	PL18+DESI	$> 2.40$	$0.628 \pm 0.057$	$0.803 \pm 0.013$	$69.21 \pm 0.48$	$0.297 \pm 0.006$	$0.467 \pm 0.035$	-0.69
	PL18+DESI+PP&SH0ES	$> 2.37$	$0.634 \pm 0.057$	$0.808 \pm 0.013$	$69.40 \pm 0.44$	$0.295 \pm 0.005$	$0.469 \pm 0.035$	-1.08
$\gamma\Lambda_s\text{CDM}(z_{\dagger} = 1.7)$	PL18	[1.7]	$0.602 \pm 0.059$	$0.771 \pm 0.014$	$73.20 \pm 1.00$	$0.264 \pm 0.011$	$0.448 \pm 0.036$	4.41
	PL18+ $f\sigma_8$	[1.7]	$0.586 \pm 0.022$	$0.774 \pm 0.011$	$73.06 \pm 0.73$	$0.265 \pm 0.007$	$0.461 \pm 0.015$	1.97
$\gamma\Lambda_s\text{CDM}(z_{\dagger} = 2.16)$	PL18+ $f\sigma_8$ +PP&SH0ES	[2.16]	$0.608 \pm 0.023$	$0.793 \pm 0.008$	$70.49 \pm 0.51$	$0.286 \pm 0.006$	$0.467 \pm 0.014$	-4.28
$\gamma\Lambda\text{CDM}$	PL18	-	$0.662 \pm 0.063$	$0.808 \pm 0.012$	$68.07 \pm 0.68$	$0.305 \pm 0.009$	$0.456 \pm 0.035$	-
	PL18+ $f\sigma_8$	-	$0.639 \pm 0.025$	$0.814 \pm 0.009$	$67.89 \pm 0.50$	$0.308 \pm 0.007$	$0.471 \pm 0.015$	-
	PL18+ $f\sigma_8$ +PP	-	$0.640 \pm 0.024$	$0.818 \pm 0.008$	$67.66 \pm 0.47$	$0.311 \pm 0.006$	$0.473 \pm 0.014$	-
	PL18+ $f\sigma_8$ +PP&SH0ES	-	$0.636 \pm 0.024$	$0.807 \pm 0.008$	$68.29 \pm 0.45$	$0.303 \pm 0.006$	$0.468 \pm 0.014$	-
	PL18+ $f\sigma_8$ +PP+SDSS	-	$0.636 \pm 0.025$	$0.815 \pm 0.007$	$67.82 \pm 0.39$	$0.309 \pm 0.005$	$0.473 \pm 0.014$	-
	PL18+ $f\sigma_8$ +PP+DESI	-	$0.637 \pm 0.025$	$0.808 \pm 0.006$	$68.19 \pm 0.37$	$0.304 \pm 0.005$	$0.468 \pm 0.014$	-
	PL18+DESI	-	$0.693^{+0.060}_{-0.051}$	$0.795 \pm 0.007$	$68.63 \pm 0.44$	$0.298 \pm 0.006$	$0.432 \pm 0.029$	-
	PL18+DESI+PP&SH0ES	-	$0.701^{+0.061}_{-0.047}$	$0.791 \pm 0.007$	$68.83 \pm 0.41$	$0.296 \pm 0.005$	$0.426 \pm 0.029$	-

in the analysis, the inferred value of  $\gamma$  across different datasets consistently yields  $\gamma \sim 0.638$ , as seen in Table II and Figs. 1 and 2. In the analyses that do not include  $f\sigma_8$  data, we observe relatively higher mean values of  $\gamma$ , with this effect being particularly pronounced for the PL18+DESI and PL18+DESI+PP&SH0ES combinations (see Fig. 2). However, since the uncertainties on  $\gamma$  in these cases do not improve significantly compared to the Planck-alone analysis, the  $\gamma$  tension worsens relative to the PL18 case but remains below  $3\sigma$ , in contrast to dataset combinations that include the  $f\sigma_8$  likelihood, where the tension consistently exceeds  $3\sigma$ . Correspondingly,  $H_0$  and  $\Omega_{m0}$  remain robustly consistent with their Planck-alone predictions— $H_0 = 68.07 \pm 0.68 \text{ km s}^{-1} \text{ Mpc}^{-1}$  and  $\Omega_{m0} = 0.305 \pm 0.009$ —within  $1\sigma$ . These values are also closely aligned with the standard Planck- $\Lambda\text{CDM}$  model [36].

We see that the present-day growth rate,  $f_0 = \Omega_{m0}^{\gamma}$ , remains largely unchanged across all dataset combinations for  $\gamma\Lambda\text{CDM}$  and closely matches that of  $\gamma\Lambda_s\text{CDM}$  in most cases. Notable exceptions arise for PL18 and PL18+DESI, where  $\gamma\Lambda\text{CDM}$  yields modestly lower  $f_0$  values. This suggests that in  $\gamma\Lambda\text{CDM}$ , the late-time growth suppression is achieved primarily by increasing  $\gamma$  beyond its GR-predicted value of 0.55, rather than by lowering  $\Omega_{m0}$ . Consequently, in  $\gamma\Lambda\text{CDM}$ , the  $H_0$  value remains anchored near the Planck-likelihood baseline,  $H_0 = 68.07 \pm 0.68 \text{ km s}^{-1} \text{ Mpc}^{-1}$ , failing to reconcile the SH0ES

measurement of  $H_0 = 73.04 \pm 1.04 \text{ km s}^{-1} \text{ Mpc}^{-1}$  [165].

The  $\gamma\Lambda_s\text{CDM}$  model addresses the late-time growth suppression by lowering  $\Omega_{m0}$  (and consequently increasing  $H_0$ ), rather than elevating the growth-index  $\gamma$  to values around 0.64, as is clearly seen in the  $\Omega_{m0}$ - $\gamma$  contours of Fig. 1. We observe from Table II that  $\Omega_{m0}$  in  $\gamma\Lambda_s\text{CDM}$  is systematically lower by  $\sim 0.02$ – $0.05$  compared to  $\gamma\Lambda\text{CDM}$ . Despite this difference, the present-day growth rate,  $f_0 = \Omega_{m0}^{\gamma}$ , remains nearly identical in both models, meaning the final suppression of structure growth is comparable—but crucially,  $\gamma\Lambda_s\text{CDM}$  achieves this without requiring  $\gamma$  to exceed 0.6 significantly. As a result, Table III demonstrates that  $\gamma\Lambda_s\text{CDM}$  simultaneously reduces the  $\gamma$  and  $H_0$  tensions—often by predicting  $S_8 \sim 0.80$  values consistently lower than that of Planck- $\Lambda\text{CDM}$  ( $S_8 = 0.832 \pm 0.013$  [36]) and aligning with Planck- $\Lambda_s\text{CDM}$  ( $S_8 = 0.801^{+0.026}_{-0.016} \pm 0.013$  [43, 45])—to approximately the  $2$ – $3\sigma$  level, rather than leaving them at  $3.8$ – $4.7\sigma$ . The close agreement in  $f_0$  between the two models, despite their stark differences in  $\Omega_{m0}$  and  $\gamma$ , aligns directly with the mechanism outlined in Section II, which was anticipated to simultaneously address the  $\gamma$ ,  $H_0$ , and  $S_8$  tensions.

As shown in Table III, the  $\gamma\Lambda_s\text{CDM}$  model exhibits good performance in alleviating the  $H_0$  tension, mirroring the standard ( $\gamma = 0.55$ )  $\Lambda_s\text{CDM}$  framework [41–43, 45, 46]. In particular, for the Planck-alone and PL18+ $f\sigma_8$  analyses, both of which yield a lower

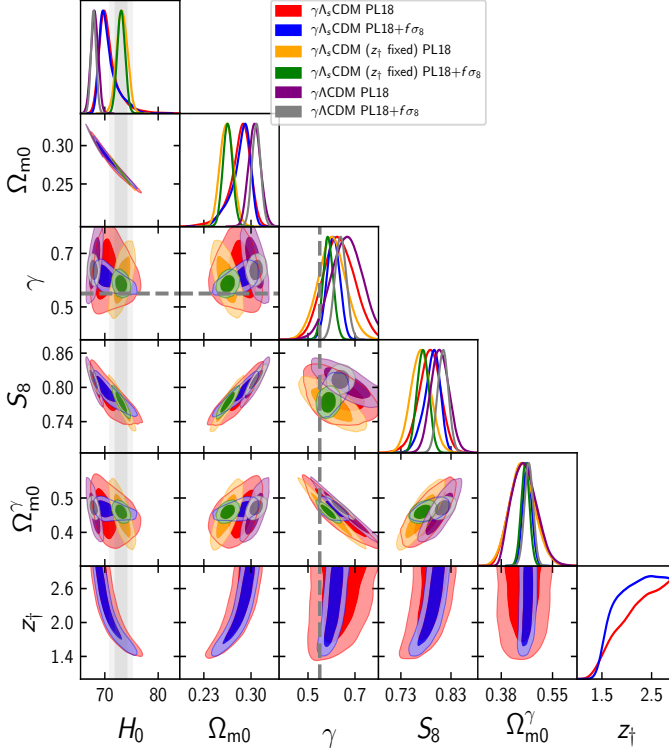


FIG. 1. Triangle plot for the likelihoods PL18 and PL18+ $f\sigma_8$  for the models  $\gamma\Lambda$ CDM,  $\gamma\Lambda_s$ CDM, and  $\gamma\Lambda_s$ CDM with  $z_{\dagger} = 1.7$ . The gray dotted line represents the theoretical value  $\gamma = 0.55$ , and the gray band represents the value  $H_0 = 73.04 \pm 1.04 \text{ km s}^{-1} \text{ Mpc}^{-1}$  found by the SH0ES collaboration.

bound of  $z_{\dagger} > 1.6$  for the mirror AdS-to-dS transition redshift, the  $H_0$  tension drops below  $1.5\sigma$ , with values of  $H_0 = 70.76^{+0.72}_{-2.1} \text{ km s}^{-1} \text{ Mpc}^{-1}$  and  $H_0 = 70.67^{+0.72}_{-2.0} \text{ km s}^{-1} \text{ Mpc}^{-1}$ , respectively, though we note the relatively larger uncertainties and non-Gaussianities in the posteriors and refer the reader to Fig. 1 for the marginalized posteriors. The improvement in the  $\gamma$  tension follows a similar trend, with the Planck-alone analysis yielding  $\gamma = 0.631 \pm 0.065$ , corresponding to a  $1.2\sigma$  tension with the theoretically expected value, while the PL18+ $f\sigma_8$  combination gives  $\gamma = 0.607 \pm 0.027$ , corresponding to a  $2.1\sigma$  tension. We emphasize that in the Planck-alone case, the relatively larger uncertainties contribute to the reduced significance of the  $\gamma$  tension. Additionally, we note that  $S_8 \approx 0.79$  remains consistent with the predictions of the standard Planck- $\Lambda_s$ CDM and KiDS- $\Lambda_s$ CDM analyses [43, 45], implying that our results do not indicate deviations from the standard  $\Lambda_s$ CDM framework. Incorporating SN Ia data further strengthens the constraints. In the PL18+ $f\sigma_8$ +PP case, the lower bound on the transition redshift increases slightly to  $z_{\dagger} > 2.12$ , diminishing the impact of the mirror AdS-to-dS transition. Consequently, both the  $H_0$  and  $\gamma$  tensions increase to  $\sim 3.1\sigma$ , but this still constitutes a non-negligible improvement over  $\gamma\Lambda$ CDM, which exhibits a  $3.8\sigma$   $\gamma$  tension and a  $4.7\sigma$   $H_0$  tension for the same dataset combination. In contrast,

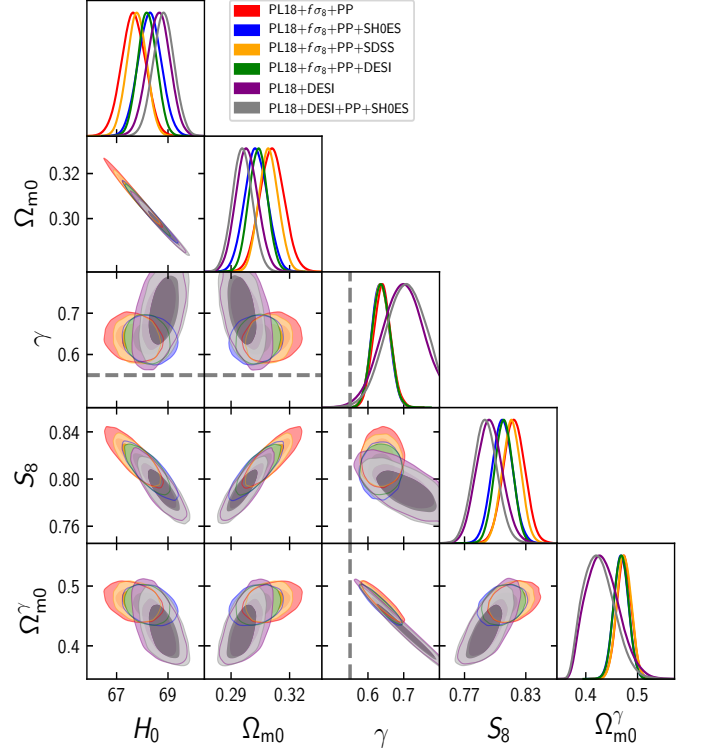


FIG. 2. Marginalized posterior distributions arranged on a triangle plot for  $\gamma\Lambda$ CDM. The gray dotted line represents the theoretical value  $\gamma = 0.55$ . The only case where this value falls within the  $2\sigma$  contour is when the PL18 likelihood is used alone, as seen in Fig. 1; any other data combination is in tension with it at a level of at least  $2\sigma$ .

for the PL18+ $f\sigma_8$ +PP&SH0ES combination, the lower bound on  $z_{\dagger}$  does not increase significantly relative to the Planck-alone analysis, allowing the model to operate more effectively. This results in a reduction of both the  $\gamma$  and  $H_0$  tensions, bringing them down to  $2.4\sigma$  and  $1.9\sigma$ , respectively, below the commonly considered  $2.5\sigma$  threshold for a tension to be statistically significant. Moreover, it is worth noting that  $S_8 \approx 0.80$  remains consistent with the predictions of the standard Planck- $\Lambda_s$ CDM and KiDS- $\Lambda_s$ CDM analyses [43, 45].

We note that across these dataset combinations, the constraints on  $f_0 = \Omega_{m0}^{\gamma}$  remain consistent with each other within the  $1\sigma$  confidence level, as well as with those obtained for the  $\gamma\Lambda$ CDM model. This consistency leads to the positive correlation observed between  $\Omega_{m0}$  and  $\gamma$  in the  $\gamma\Lambda_s$ CDM model, as seen in the 2D contour plots of  $\Omega_{m0}$ - $\gamma$  in Figs. 1, 3 and 4. Furthermore, we also observe a negative correlation between  $\Omega_{m0}$  and  $H_0$ , as well as between  $H_0$  and  $\gamma$ , in the same figures. This highlights the key mechanism through which  $\gamma\Lambda_s$ CDM mitigates both the  $H_0$  and  $\gamma$  tensions. Specifically,  $\Omega_{m0}$  is systematically lower than in  $\gamma\Lambda$ CDM, tending to remain between 0.28 and 0.30 in all these cases, whereas in  $\gamma\Lambda$ CDM, it remains above 0.30. Notably, lower values of  $\Omega_{m0}$  in  $\gamma\Lambda_s$ CDM correlate with reduced  $\gamma$  and  $H_0$  tensions, with the most

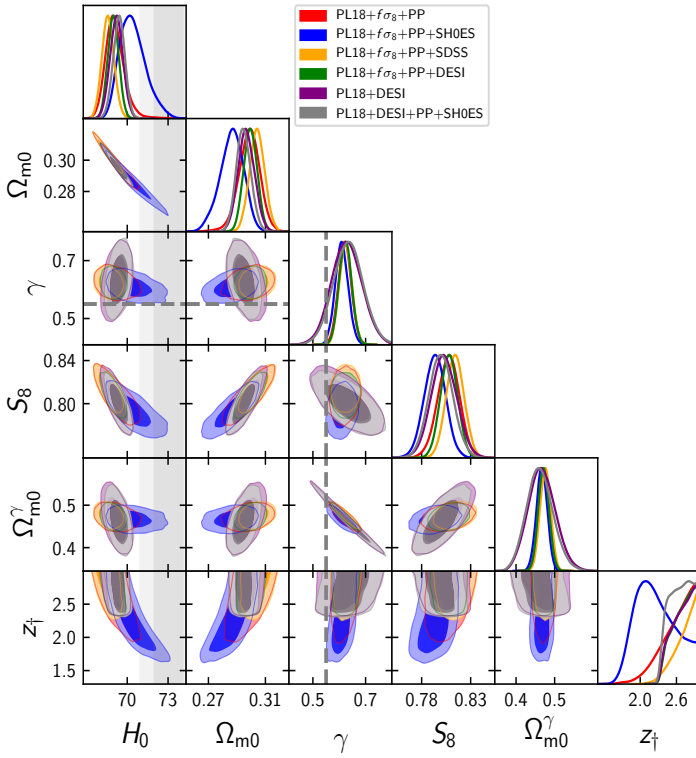


FIG. 3. Marginalized posterior distributions arranged on a triangle plot for  $\gamma\Lambda_s\text{CDM}$ . The gray dotted line represents the theoretical value  $\gamma = 0.55$ , and the gray band represents the value  $H_0 = 73.04 \pm 1.04 \text{ km s}^{-1} \text{ Mpc}^{-1}$  found by the SH0ES collaboration.

significant alleviation occurring for  $\Omega_{m0}$  values closer to 0.28 in these dataset combinations.

A closer examination of Figs. 1, 3 and 4 reveals that  $\Omega_{m0}$ ,  $\gamma$ , and  $S_8$  exhibit positive correlations with  $z_t$ , while  $H_0$  exhibits a negative correlation with it. However, these effects become noticeable only for  $z_t \lesssim 2.5$  and significant for  $z_t \lesssim 2.0$ . This is in full agreement with prior studies of  $\Lambda_s\text{CDM}$ , which anticipate that if the mirror AdS-to-dS transition occurs too early, say for  $z_t > 2.5$ , during the epoch when matter still dominates cosmic dynamics, the AdS-like CC lacks sufficient time and influence to induce meaningful deviations from the standard  $\Lambda\text{CDM}$  expansion history [41–43, 45, 46]. Indeed, we find that when  $z_t \lesssim 2.0$ , the mirror AdS-to-dS transition effectively brings both the  $\gamma$  and  $H_0$  tensions below  $\sim 2\sigma$ . Conversely, for  $z_t \gtrsim 2.5$ , the model effectively converges toward  $\gamma\Lambda\text{CDM}$ , compromising its ability to mitigate the  $\gamma$  and  $H_0$  tensions and offering only marginal improvements over  $\gamma\Lambda\text{CDM}$ .

This behavior is particularly evident when we extend the combined PL18+ $f\sigma_8$ +PP dataset by incorporating BAO data, either from SDSS or DESI. We find that PL18+ $f\sigma_8$ +PP+SDSS yields  $z_t > 2.3$  and PL18+ $f\sigma_8$ +PP+DESI gives  $z_t > 2.4$ , placing both cases in the regime where the transition redshift is too high to fully resolve the tensions. As a result, as seen in Table III,

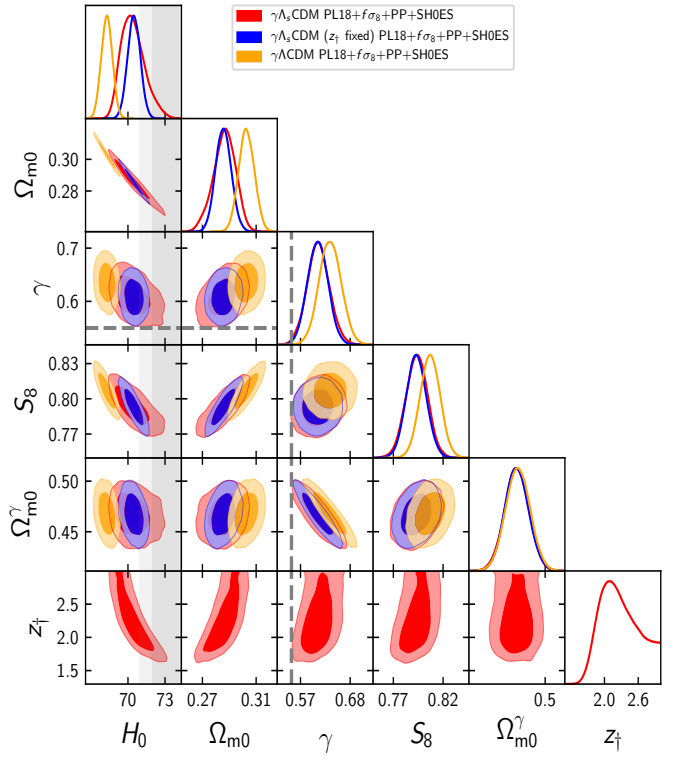


FIG. 4. Triangle plot for the likelihood PL18+ $f\sigma_8$ +PP+SH0ES for the models  $\gamma\Lambda\text{CDM}$ ,  $\gamma\Lambda_s\text{CDM}$ , and  $\gamma\Lambda_s\text{CDM}$  with  $z_t = 2.16$ . The gray dotted line represents the theoretical value of  $\gamma = 0.55$ , and the gray band represents the value of  $H_0 = 73.04 \pm 1.04 \text{ km s}^{-1} \text{ Mpc}^{-1}$  found by the SH0ES collaboration.

$\gamma\Lambda_s\text{CDM}$  provides only modest improvements: the  $\gamma$  tension remains at approximately  $3.0\sigma$  for both cases, while the  $H_0$  tension is at the  $3.6\sigma$  and  $3.9\sigma$  levels, respectively. Nevertheless, these results indicate that  $\gamma\Lambda_s\text{CDM}$  still performs  $\sim 0.4\sigma$  better than  $\gamma\Lambda\text{CDM}$  in alleviating the  $\gamma$  tension and  $\sim 0.8\sigma$  better in reducing the  $H_0$  tension.

We observe that in the case of the PL18+ $f\sigma_8$ +PP+DESI combination,  $\gamma\Lambda_s\text{CDM}$  performs slightly better than in PL18+ $f\sigma_8$ +PP+SDSS in mitigating both the  $\gamma$  and  $H_0$  tensions. Moreover, when comparing the minimum  $\chi^2_{\min}$  values, we find that  $\gamma\Lambda_s\text{CDM}$  provides a worse fit to the PL18+ $f\sigma_8$ +PP+SDSS dataset than  $\gamma\Lambda\text{CDM}$ , yielding  $\Delta\chi^2_{\min} = 3.21$ . However, for the PL18+ $f\sigma_8$ +PP+DESI dataset,  $\gamma\Lambda_s\text{CDM}$  fits better than  $\gamma\Lambda\text{CDM}$ , with  $\Delta\chi^2_{\min} = -1.18$ . Given this, we conducted further analysis using the DESI BAO dataset, specifically studying the cases PL18+DESI and PL18+DESI+PP&SH0ES. In both cases,  $\gamma\Lambda_s\text{CDM}$  fits the data slightly better than  $\gamma\Lambda\text{CDM}$  and yields a lower bound on  $z_t$  of  $z_t > 2.4$ . In the PL18+DESI case, with  $\gamma = 0.628 \pm 0.057$ ,  $\gamma\Lambda_s\text{CDM}$  mitigates the  $\gamma$  tension, reducing it to  $\sim 1.4\sigma$ , while the  $H_0$  tension is only moderately alleviated, remaining at  $\sim 3.3\sigma$ . The improvement in the  $\gamma$  tension is largely attributed to the relatively large uncertainty



TABLE III. Significance of the  $H_0$  and  $\gamma$  tensions across extended combinations of datasets. We assume  $\gamma = 0.55$  for both models and incorporate the SH0ES  $H_0$  measurement.

Model	Data	$\sigma_\gamma$	$\sigma_{H_0}$
$\gamma\Lambda_s\text{CDM}(z_\dagger \text{ free})$	PL18	1.2 $\sigma$	1.3 $\sigma$
	PL18+ $f\sigma_8$	2.1 $\sigma$	1.4 $\sigma$
	PL18+ $f\sigma_8$ +PP	3.0 $\sigma$	3.2 $\sigma$
	PL18+ $f\sigma_8$ +PP&SH0ES	2.4 $\sigma$	1.9 $\sigma$
	PL18+ $f\sigma_8$ +PP+SDSS	3.1 $\sigma$	3.9 $\sigma$
	PL18+ $f\sigma_8$ +PP+DESI	3.0 $\sigma$	3.6 $\sigma$
	PL18+DESI	1.4 $\sigma$	3.3 $\sigma$
	PL18+DESI+PP&SH0ES	1.5 $\sigma$	3.2 $\sigma$
$\gamma\Lambda_s\text{CDM}(z_\dagger = 1.7)$	PL18	0.9 $\sigma$	0.1 $\sigma$
	PL18+ $f\sigma_8$	1.6 $\sigma$	0.0 $\sigma$
$\gamma\Lambda_s\text{CDM}(z_\dagger = 2.16)$	PL18+ $f\sigma_8$ +PP&SH0ES	2.2 $\sigma$	1.8 $\sigma$
$\gamma\Lambda\text{CDM}$	PL18	1.8 $\sigma$	4.0 $\sigma$
	PL18+ $f\sigma_8$	3.6 $\sigma$	4.5 $\sigma$
	PL18+ $f\sigma_8$ +PP	3.8 $\sigma$	4.7 $\sigma$
	PL18+ $f\sigma_8$ +PP&SH0ES	3.6 $\sigma$	4.2 $\sigma$
	PL18+ $f\sigma_8$ +PP+SDSS	3.4 $\sigma$	4.7 $\sigma$
	PL18+ $f\sigma_8$ +PP+DESI	3.5 $\sigma$	4.4 $\sigma$
	PL18+DESI	2.6 $\sigma$	3.9 $\sigma$
	PL18+DESI+PP&SH0ES	2.8 $\sigma$	3.8 $\sigma$

in the constraint on  $\gamma$  in this dataset combination. In contrast, with  $\gamma = 0.693^{+0.060}_{-0.051}$ ,  $\gamma\Lambda\text{CDM}$ , despite having similarly large uncertainties, exhibits a significantly higher  $\gamma$  tension at the 2.6 $\sigma$  level, while also yielding a 3.6 $\sigma$   $H_0$  tension. This suggests that even when  $z_\dagger$  is constrained to relatively high values,  $\gamma\Lambda_s\text{CDM}$  continues to offer a modest advantage over  $\gamma\Lambda\text{CDM}$  in alleviating cosmological tensions, particularly in the context of the  $\gamma$  tension. However, since the DESI BAO data constrain  $z_\dagger$  to relatively high values ( $z_\dagger > 2.4$ ), the ability of  $\gamma\Lambda_s\text{CDM}$  to fully resolve both the  $H_0$  and  $\gamma$  tensions is somewhat limited in this dataset combination. Notably, this picture remains unchanged when SN Ia data are included in the analysis, as we find similar results for PL18+DESI+PP&SH0ES.

These higher tensions, which arise when the BAO data are incorporated into our analysis, suggest that the DESI and SDSS datasets—both of which rely on 3D BAO measurements calibrated against Planck- $\Lambda\text{CDM}$  as the fiducial model—limit the effectiveness of  $\gamma\Lambda_s\text{CDM}$  in predicting  $\gamma = 0.55$ .<sup>3</sup> Even so, the DESI likelihood still shows a slight preference for  $\gamma\Lambda_s\text{CDM}$ , as indicated by its nega-

tive  $\Delta\chi^2_{\min}$  value. Moreover, in all analyses incorporating DESI data,  $\gamma\Lambda_s\text{CDM}$  consistently reduces both the  $H_0$  and  $\gamma$  tensions by approximately 0.5–1 $\sigma$  compared to  $\gamma\Lambda\text{CDM}$  for the same dataset combinations.

As a next step, we fix  $z_\dagger = 1.7$ , motivated by previous studies on  $\Lambda_s\text{CDM}$  showing that a mirror AdS-to-dS transition around this redshift effectively alleviates multiple major cosmological tensions, including those in  $H_0$ ,  $M_B$ , and  $S_8$  [41–43, 45]. For instance, Ref. [43] finds  $z_\dagger = 1.72^{+0.09}_{-0.12}$  from a combined analysis using Planck+BAOtr+PP&SH0ES+KiDS-1000, yielding  $H_0 = 73.16 \pm 0.64 \text{ km s}^{-1} \text{ Mpc}^{-1}$  and completely eliminating the  $H_0$  tension. For this reason, we find it interesting to explicitly examine the  $z_\dagger = 1.7$  scenario, for the Planck-alone and PL18+ $f\sigma_8$  dataset combinations, as our free  $z_\dagger$  analysis indicates that  $z_\dagger = 1.7$  remains consistent with the lower bound  $z_\dagger > 1.58$  inferred for these cases. Thus, for these cases, we conduct an additional analysis of the  $\gamma\Lambda_s\text{CDM}$  model by fixing  $z_\dagger = 1.7$ , reducing the number of free parameters to the same seven as  $\gamma\Lambda\text{CDM}$ , and evaluating its impact on the inferred cosmological tensions. As seen in Tables II and III, this special case can effectively eliminate both the  $\gamma$  and  $H_0$  tensions in each of these two data combinations. See also Fig. 1, which compares PL18 and PL18+ $f\sigma_8$  for  $\gamma\Lambda\text{CDM}$ ,  $\gamma\Lambda_s\text{CDM}$ , and the special fixed- $z_\dagger = 1.7$  case. However, this value of  $z_\dagger$  is disfavored by both the PL18 and PL18+ $f\sigma_8$  in terms of goodness of fit, as the  $\gamma\Lambda_s\text{CDM}$  model worsens the  $\chi^2_{\min}$  by  $\sim 4$  and  $\sim 2$ , respectively, compared to  $\gamma\Lambda\text{CDM}$ . Moreover, in our analyses including any other data set, this value of  $z_\dagger$  is excluded at more than 2 $\sigma$ . Regardless, in the Planck-alone analysis, the lowered  $\Omega_{m0}$  implied by  $z_\dagger = 1.7$  raises  $H_0$  enough to remove the  $H_0$  tension completely (0.1 $\sigma$ ) and simultaneously keeps  $\gamma$  near 0.55, eliminating the  $\gamma$  tension (0.9 $\sigma$ ) as well. A similar effect emerges when  $f\sigma_8$  data are added: the PL18+ $f\sigma_8$  combination still allows  $H_0$  to remain sufficiently high ( $\gtrsim 73 \text{ km s}^{-1} \text{ Mpc}^{-1}$ ) while keeping  $\gamma \approx 0.58\text{--}0.60$ , reducing the  $\gamma$  tension to 1.6 $\sigma$  and driving the  $H_0$  tension down to 0 $\sigma$ . The fact that

has been shown that when combined with CMB data, the overall fit remains comparable to, or even slightly better than, standard  $\Lambda\text{CDM}$  in terms of Bayesian evidence [42]. A detailed analysis in [42] demonstrated that low- $z$  SDSS BAO data primarily weaken the model's success, whereas high- $z$  BAO, viz., Ly- $\alpha$  BAO, favor a transition redshift of  $z_\dagger \lesssim 2.3$ . Recognizing that high- $z$  and low- $z$  BAO constraints yield distinctive correlations in the  $H_0$ - $\Omega_{m0}$  plane within  $\Lambda\text{CDM}$  [163], Ref. [45] performed an analysis using only the high- $z$  subset of SDSS BAO data ( $z > 1$ ), finding that both the model's fit and its ability to mitigate cosmological tensions improve significantly compared to using the full SDSS BAO dataset. Furthermore, Ref. [43] investigated the use of transverse BAO (BAOtr) (or 2D BAO), a less model-dependent alternative to the commonly used 3D BAO data (often referred to simply as BAO), which relies on Planck- $\Lambda\text{CDM}$  to determine the distance to the spherical shell and could potentially introduce a bias when analyzing scenarios beyond  $\Lambda\text{CDM}$ . They found that combining Planck with BAOtr provides very strong Bayesian evidence for  $\Lambda_s\text{CDM}$  over  $\Lambda\text{CDM}$ , yielding  $H_0 = 73.30^{+1.20}_{-1.00} \text{ km s}^{-1} \text{ Mpc}^{-1}$  and completely eliminating the  $H_0$  tension.

<sup>3</sup> The performance of the abrupt  $\Lambda_s\text{CDM}$  model against pre-DESI BAO data, particularly the SDSS BAO dataset, has been extensively studied in the literature [41, 42, 45]. While SDSS BAO data statistically favors  $z_\dagger \gtrsim 2.1$ , limiting the model's effectiveness, it



$\gamma\Lambda_s\text{CDM}$  with  $z_{\dagger} = 1.7$  can completely drive down both tensions to  $\lesssim 1\sigma$  for PL18 and PL18+ $f\sigma_8$  underscores the key role of a rapid mirror AdS-to-dS transition at  $z_{\dagger} \approx 1.7$  for jointly alleviating the  $H_0$  and  $\gamma$  tensions. This corroborates earlier findings in standard ( $\gamma = 0.55$ ) abrupt  $\Lambda_s\text{CDM}$  studies [41–43, 45, 46], which identify  $z_{\dagger} \approx 1.7$  as the sweet spot where the major cosmological tensions—in  $H_0$ ,  $M_B$ , and  $S_8$ —are simultaneously eliminated.

Finally, another special case in our analysis focuses on the PL18+ $f\sigma_8$ +PP&SH0ES dataset, for which Table II shows that  $\gamma\Lambda_s\text{CDM}$  is strongly favored over  $\gamma\Lambda\text{CDM}$  by  $\Delta\chi^2_{\min} = -4.7$ . In this scenario, both the  $\gamma$  and  $H_0$  tensions drop significantly. Noting that the best-fit transition redshift for this combination is  $z_{\dagger} \approx 2.16$  (see Fig. 3), we fix  $z_{\dagger} = 2.16$  (removing one degree of freedom) and re-run the inference. This case yields  $\Delta\chi^2_{\min} = -4.3$ , and its comparison with  $\gamma\Lambda_s\text{CDM}$  and  $\gamma\Lambda\text{CDM}$  is provided in Fig. 4. The resulting constraints remain consistent with those found when  $z_{\dagger}$  was free to vary, except that  $H_0$  and  $\Omega_{m0}$  become more tightly constrained due to the removed degeneracy with  $z_{\dagger}$  after fixing its value. Consequently, the  $H_0$  tension is reduced to  $\sim 2.2\sigma$ , while the  $\gamma$  tension is  $\sim 2.5\sigma$ , underscoring the advantage of  $\gamma\Lambda_s\text{CDM}$  in mitigating both tensions in this best-fit scenario.

These results confirm the heuristic argument from Section II: in  $\gamma\Lambda_s\text{CDM}$ , the AdS-like CC at  $z > z_{\dagger}$  reduces  $\Omega_{m0}$ , thereby achieving the same low-redshift growth suppression ( $f_0 \approx 0.48$ ) without requiring  $\gamma > 0.6$ . The key distinction is that  $\gamma\Lambda_s\text{CDM}$  accomplishes this by lowering  $\Omega_{m0}$ , which in turn raises  $H_0$  to approximately  $70\text{--}71\text{ km s}^{-1}\text{ Mpc}^{-1}$ , thereby mitigating both the Hubble and growth tensions simultaneously. In contrast,  $\gamma\Lambda\text{CDM}$  maintains a higher  $\Omega_{m0}$ , necessitating an inflated  $\gamma \sim 0.64$  (Table II) to match  $f_0 \approx 0.48$ , which leaves the  $H_0$  tension at  $3.8\text{--}4.7\sigma$ . Furthermore, the lower present-day matter density values that drive the alleviation of both the  $\gamma$  and  $H_0$  tensions in  $\gamma\Lambda_s\text{CDM}$  also keep  $S_8$  below  $\approx 0.80$ , since  $S_8 \propto \sqrt{\Omega_{m0}}$ . This brings  $S_8$  closer to its cosmic shear constraints, as found using the KiDS-1000 data for the abrupt  $\Lambda_s\text{CDM}$  model [43, 45], indicating that the  $S_8$  tension does not arise in this model. Thus, the results in Tables II and III, together with Figs. 1–4, favor the mirror AdS-to-dS (sign-switching cosmological constant  $\Lambda_s$ ) in  $\gamma\Lambda_s\text{CDM}$  over  $\gamma\Lambda\text{CDM}$  for resolving late-time tensions. By preserving a theoretically motivated  $\gamma \approx 0.55$  while simultaneously raising  $H_0$  to match local measurements,  $\gamma\Lambda_s\text{CDM}$  naturally accounts for the observed growth suppression ( $f_0 \approx 0.48$ ) through a lower present-day matter density,  $\Omega_{m0}$ . This implies that, treating  $\gamma$  as a free parameter, the cosmological data sets used in this work all prefer a suppressed growth of structure compared to the theoretical predictions for both  $\gamma\Lambda\text{CDM}$  and  $\gamma\Lambda_s\text{CDM}$  models, however, this preference encapsulated in the deviation from the theoretical  $\gamma \approx 0.55$  value are reduced (reaching up to  $1.5\sigma$  amelioration depending on the data set combination) for  $\gamma\Lambda_s\text{CDM}$ , implying the  $\Lambda_s\text{CDM}$  framework has better consistency with its underlying theory compared to  $\Lambda\text{CDM}$ . Thus, the rapid

mirror AdS-to-dS transition in the late universe, at  $z_{\dagger} \sim 2$ , emerges as an elegant mechanism capable of addressing the Hubble,  $S_8$ , and  $\gamma$  tensions within a single, minimal extension to the standard cosmological model.

## V. CONCLUSIONS

The recently identified growth-index ( $\gamma$ ) tension [31] adds another major discrepancy to the persistent challenges facing the  $\Lambda\text{CDM}$  model—namely, the  $\sim 5\sigma$   $H_0$  tension and the  $\sim 3\sigma$   $S_8$  tension. The  $\gamma$  tension, persisting at the  $3\text{--}4\sigma$  level, arises when  $\gamma$  is treated as a free parameter in  $\Lambda\text{CDM}$ , its inferred value,  $\gamma \simeq 0.63$ , along with  $\Omega_{m0} \sim 0.32$ , significantly deviates from the theoretically expected  $\gamma \approx 0.55$  under GR. This elevated  $\gamma$  value corresponds to a suppressed growth rate of  $f_0 \simeq 0.48$ , compared to the expected  $f_0 \simeq 0.53$  for  $\gamma \approx 0.55$ , further reinforcing the deviation from  $\Lambda\text{CDM}$  [31]. The  $\Lambda_s\text{CDM}$  framework, characterized by a rapid mirror AdS-to-dS transition—where the cosmological constant  $\Lambda_s$  switches sign—at redshift  $z_{\dagger} \sim 2$ , has emerged as a promising and economical extension of  $\Lambda\text{CDM}$ , offering a unified resolution to major cosmological tensions, including those in  $H_0$ ,  $M_B$ , and  $S_8$ , while also predicting the age of the universe and, when treated as free parameters, standard neutrino properties, all within a single theoretical framework [40–46]. Robust observational analyses indicate that  $\Lambda_s\text{CDM}$  generally predicts a lower late-time matter density parameter than  $\Lambda\text{CDM}$ ; specifically, Planck- $\Lambda_s\text{CDM}$  yields  $\Omega_{m0} \simeq 0.28$ , which, when combined with the theoretically expected growth index  $\gamma \approx 0.55$  [147] under GR, leads to  $f_0 \simeq 0.49$ , in close agreement with [31]. Furthermore, previous studies have shown that for  $z_{\dagger} \approx 1.7$ ,  $\Lambda_s\text{CDM}$  resolves both the  $H_0$  and  $S_8$  tensions, bringing them below  $\sim 1\sigma$  [43] by predicting  $\Omega_{m0} \approx 0.27$ , which in turn yields  $f_0 = 0.48$ , in precise agreement with Ref. [31]. Thus, we conclude that the  $\Lambda_s\text{CDM}$  framework presents a compelling possibility for a unified resolution of major cosmological tensions, including the recently identified  $\gamma$  tension, through a single underlying physical mechanism. Accordingly, we rigorously examined this potential by adopting the *abrupt*  $\Lambda_s\text{CDM}$  scenario as a proxy for rapid transitions, under the assumption that gravity is governed by GR. Following the methodology of Ref. [31], we performed a systematic parameter inference analysis, first using Planck-alone (PL18) and PL18+ $f\sigma_8$  datasets, then extending our study to additional datasets—including SN Ia (PantheonPlus with/without SH0ES) and BAO (SDSS, DESI)—to assess the robustness of  $\gamma\Lambda_s\text{CDM}$  across different cosmological probes.

Our analysis confirms this expectation: the  $\Lambda_s\text{CDM}$  framework offers a unified mechanism that simultaneously addresses the  $\gamma$ ,  $H_0$ , and  $S_8$  tensions. A key observation is that, despite their fundamental differences,  $\gamma\Lambda_s\text{CDM}$  and  $\gamma\Lambda\text{CDM}$  yield nearly identical present-day growth rates,  $f_0 = \Omega_{m0}^{\gamma}$ , across all dataset combinations. However, they achieve this through distinct mechanisms:  $\gamma\Lambda\text{CDM}$  sup-

presses structure growth by increasing  $\gamma$  to  $\sim 0.63$  while maintaining a high  $\Omega_{m0} > 0.3$ , exacerbating the  $\gamma$  tension. In contrast,  $\gamma\Lambda_s\text{CDM}$  is better at preserving the theoretically expected  $\gamma \approx 0.55$  by lowering  $\Omega_{m0}$  by  $\sim 0.02\text{--}0.05$ , which also naturally raises  $H_0$ , without deviating from the standard  $\Lambda_s\text{CDM}$  framework as significantly as  $\gamma\Lambda\text{CDM}$  does from  $\Lambda\text{CDM}$ . This distinction is evident in the  $\Omega_{m0}\text{--}\gamma$  contours, where  $\gamma\Lambda_s\text{CDM}$  exhibits a strong positive correlation, setting it apart from  $\gamma\Lambda\text{CDM}$ . Additionally, the lower  $\Omega_{m0}$  keeps  $S_8$  below  $\sim 0.80$ , bringing it into better agreement with cosmic shear constraints, particularly the KiDS-1000  $\Lambda_s\text{CDM}$  estimate [43, 45]. This reinforces the notion that  $\Lambda_s\text{CDM}$  is a compelling alternative to  $\Lambda\text{CDM}$ , providing a unified resolution to multiple major cosmological tensions through a single underlying mechanism: a mirror AdS-to-dS transition, or a similar phenomenon, occurring in the late universe at  $z_{\dagger} \sim 2$ .

To summarize our observational findings, we first constrained both models using the PL18 dataset alone, where the only significant tension appeared in  $\gamma\Lambda\text{CDM}$ , with the  $H_0$  tension persisting at  $\sim 3.5\sigma$ , while  $\gamma\Lambda_s\text{CDM}$  remained free of statistically significant tensions. Including the  $f\sigma_8$  data confirmed the emergence of the  $\gamma$  tension in  $\gamma\Lambda\text{CDM}$ , with  $\Omega_{m0} \approx 0.31$  and  $\gamma \approx 0.64$  at  $\sim 4\sigma$  significance, consistent with Ref. [31], while further exacerbating the  $H_0$  tension to  $\sim 4.5\sigma$ . In contrast,  $\gamma\Lambda_s\text{CDM}$ , with  $\Omega_{m0} \approx 0.28$  and  $\gamma \approx 0.61$ , substantially mitigated both tensions, reducing them to well below the  $2.5\sigma$  statistical significance threshold. When incorporating the Pantheon-Plus data, both the  $H_0$  and  $\gamma$  tensions in  $\gamma\Lambda_s\text{CDM}$  rise to  $\sim 3\sigma$ , while in  $\gamma\Lambda\text{CDM}$ , they increase only marginally at the decimal level but remain significantly higher than in  $\gamma\Lambda_s\text{CDM}$ . Nevertheless, incorporating the Pantheon-Plus&SH0ES data once again reduces both the  $H_0$  and  $\gamma$  tensions below  $2.5\sigma$  in  $\gamma\Lambda_s\text{CDM}$ , while in  $\gamma\Lambda\text{CDM}$ , both tensions persist at the  $\sim 4\sigma$  level. This case, namely PL18+ $f\sigma_8$ +PP&SH0ES, is particularly significant as it demonstrates that  $\gamma\Lambda_s\text{CDM}$  provides a statistically superior fit to the data. Consequently, fixing  $z_{\dagger}$  to its best-fit value for this dataset ( $z_{\dagger} = 2.16$ ) reduces the number of free parameters to match those of  $\gamma\Lambda\text{CDM}$ . Despite this constraint tightening, both the  $H_0$  and  $\gamma$  tensions remain statistically insignificant ( $\sim 2\sigma$ ).

When incorporating BAO data instead of SN Ia, both models exhibit a worsening of the  $H_0$  and  $\gamma$  tensions. In  $\gamma\Lambda_s\text{CDM}$ , the  $\gamma$  tension rises to  $\sim 3\sigma$ , while the  $H_0$  tension approaches  $4\sigma$ , whereas in  $\gamma\Lambda\text{CDM}$ , these tensions reach  $\sim 3.5\sigma$  and exceed  $4.5\sigma$ . The worsening of  $\gamma\Lambda_s\text{CDM}$  arises because BAO datasets push the transition redshift to  $z_{\dagger} \gtrsim 2.3$ , causing the mirror AdS-to-dS transition to occur too early—while matter still dominates cosmic dynamics—thereby preventing the AdS-like CC from inducing significant deviations from the  $\gamma\Lambda\text{CDM}$  expansion. This aligns with previous findings on abrupt  $\Lambda_s\text{CDM}$ , where 3D BAO datasets, like those used here, weaken the model’s effectiveness, in contrast to transverse (2D) BAO data, which are less model-dependent—see Footnote 3.

Interestingly, while  $\gamma\Lambda_s\text{CDM}$  provides a slightly worse

fit to SDSS BAO than  $\gamma\Lambda\text{CDM}$ , it fits DESI BAO better, suggesting that different BAO datasets respond differently to model assumptions. Motivated by this, we performed additional analyses using DESI data, specifically for PL18+DESI and PL18+DESI+PP&SH0ES. In both cases,  $\gamma\Lambda_s\text{CDM}$  provided a marginally better fit than  $\gamma\Lambda\text{CDM}$  and yielded a lower bound of  $z_{\dagger} > 2.4$ . The corresponding tensions in  $\gamma\Lambda_s\text{CDM}$  were reduced to  $1.5\sigma$  for  $\gamma$  and  $\sim 3\sigma$  for  $H_0$ , compared to  $\sim 3\sigma$  and  $4\sigma$  in  $\gamma\Lambda\text{CDM}$ . However, these improvements stem primarily from increased parameter uncertainties rather than directly validating the efficacy of the  $\Lambda_s\text{CDM}$  framework.

Finally, we examined the special case of fixing  $z_{\dagger} = 1.7$ , motivated by previous studies on abrupt  $\Lambda_s\text{CDM}$  that identified this value as a sweet spot for simultaneously resolving multiple major tensions [42, 43, 45, 46]. While  $z_{\dagger} = 1.7$  is disfavored by the dataset combinations considered in our analysis, it remains consistent with the lower bound  $z_{\dagger} > 1.58$  found for Planck-alone and PL18+ $f\sigma_8$ , which led us to focus on these two cases. In this scenario,  $\gamma\Lambda_s\text{CDM}$ , yielding  $\Omega_{m0} \approx 0.27$ , underscores the key mechanism of the model by successfully resolving both the  $\gamma$  and  $H_0$  tensions—bringing both below  $1\sigma$  for PL18 and, for PL18+ $f\sigma_8$ , reducing the  $H_0$  tension to  $0\sigma$  with  $H_0 = 73.06 \pm 0.73 \text{ km s}^{-1} \text{ Mpc}^{-1}$  and the  $\gamma$  tension to  $1.6\sigma$  with  $\gamma = 0.586 \pm 0.022$ —, indicating consistency with the standard  $\Lambda_s\text{CDM}$  framework, while keeping  $S_8 \approx 0.77$ , in full agreement with its KiDS-1000  $\Lambda_s\text{CDM}$ -inferred value [43, 45]. Although this scenario yields a statistically worse fit to the data, it serves as a compelling demonstration that the  $\Lambda_s\text{CDM}$  framework—suggesting a late-time mirror AdS-to-dS transition (or a similar phenomenon)—could potentially offer a unified resolution to the major cosmological tensions, namely the  $H_0$ ,  $S_8$ , and the recently identified  $\gamma$  tensions, through a single underlying physical mechanism.

Our current work is based on the simplest, idealized version of the  $\Lambda_s\text{CDM}$  framework—namely, the abrupt  $\Lambda_s\text{CDM}$  model—where an abrupt AdS-to-dS transition is phenomenologically adopted as a proxy for rapid cosmic evolution under the assumption that gravity is governed by GR. While this provides a clear proof of concept, a fully consistent realization of the scenario would require a smooth transition, ensuring a well-defined dynamical process rather than an instantaneous change. Beyond being a technical refinement, such an extension would introduce distinct observational signatures depending on the transition’s duration, rapidity, and functional form, potentially leaving detectable imprints on large-scale structure growth and clustering statistics. A natural phenomenological approach would involve modeling  $\Lambda_s(z)$  with smooth functions, such as hyperbolic tangents, in redshift or scale while maintaining GR. Alternatively, a more fundamental route would be to establish a concrete physical mechanism for the transition. For instance, the Ph- $\Lambda_s\text{CDM}$  model [62], which realizes a smooth  $\Lambda_s\text{CDM}$  scenario via a phantom field with a hyperbolic tanh-type potential, provides a well-motivated physical framework within GR,

where the theoretical expectation for the growth index remains  $\gamma \approx 0.55$ . Furthermore, the smooth  $\Lambda_s$ CDM framework has recently been embedded into modified gravity theories, where deviations from GR can alter the theoretically expected value of  $\gamma$ , particularly during the transition epoch. This presents an alternative direction for extending our work by systematically examining the status of the growth index tension in different physical realizations of  $\Lambda_s$ CDM. Notable examples include  $\Lambda_s$ VCDM [44, 45], which embeds  $\Lambda_s$ CDM into VCDM, a type-II minimally modified gravity, where  $\gamma$  deviations are expected primarily during the transition, and  $f(T)$ - $\Lambda_s$ CDM [61], which implements it within teleparallel  $f(T)$  gravity. There also exist theoretical realizations of the abrupt  $\Lambda_s$ CDM scenario.  $\Lambda_s$ CDM<sup>+</sup> [57–59] provides a string-inspired realization, characterized by a distinct signature—predicting a slight excess in the total effective number of neutrino species, with  $N_{\text{eff}} = 3.294$ . Additionally, it was demonstrated in [56] that in various formulations of GR, an abrupt  $\Lambda_s$  can arise naturally through an overall sign change in the metric signature.

Given the promising success of the  $\Lambda_s$ CDM framework in alleviating multiple cosmological tensions—most notably the long-standing  $H_0$  and  $S_8$  discrepancies, as demonstrated in previous studies, as well as the recently identified  $\gamma$  tension, as shown in the present work—further exploration of its theoretical foundations

and observational consequences is well motivated. If different realizations of  $\Lambda_s$ CDM continue to exhibit comparable efficacy in addressing these tensions, a systematic analysis of the growth index  $\gamma$  within these scenarios would not only assess whether they encounter a  $\gamma$  tension but also serve as a critical test for distinguishing their underlying physical mechanisms and evaluating which, if any, could outperform  $\Lambda$ CDM as a viable alternative for the standard model of cosmology.

## VI. ACKNOWLEDGMENTS

The authors thank Enrico Specogna for useful discussions. Ö.A. acknowledges the support of the Turkish Academy of Sciences in the scheme of the Outstanding Young Scientist Award (TÜBA-GEBİP). E.D.V. is supported by a Royal Society Dorothy Hodgkin Research Fellowship. J.A.V. acknowledges the support provided by UNAM-DGAPA-PAPIIT IN117723, the award Cátedras Marcos Moshinsky. This article is based upon work from the COST Action CA21136 “Addressing observational tensions in cosmology with systematics and fundamental physics” (CosmoVerse), supported by COST (European Cooperation in Science and Technology). We acknowledge IT Services at The University of Sheffield for the provision of services for High Performance Computing.

- 
- [1] L. Verde, T. Treu, and A. G. Riess, Tensions between the Early and the Late Universe, *Nature Astron.* **3**, 891 (2019), [arXiv:1907.10625 \[astro-ph.CO\]](#).
  - [2] E. Di Valentino *et al.*, Snowmass2021 - Letter of interest cosmology intertwined II: The hubble constant tension, *Astropart. Phys.* **131**, 102605 (2021), [arXiv:2008.11284 \[astro-ph.CO\]](#).
  - [3] E. Di Valentino, O. Mena, S. Pan, L. Visinelli, W. Yang, A. Melchiorri, D. F. Mota, A. G. Riess, and J. Silk, In the realm of the Hubble tension—a review of solutions, *Class. Quant. Grav.* **38**, 153001 (2021), [arXiv:2103.01183 \[astro-ph.CO\]](#).
  - [4] L. Perivolaropoulos and F. Skara, Challenges for  $\Lambda$ CDM: An update, *New Astron. Rev.* **95**, 101659 (2022), [arXiv:2105.05208 \[astro-ph.CO\]](#).
  - [5] N. Schöneberg, G. Franco Abellán, A. Pérez Sánchez, S. J. Witte, V. Poulin, and J. Lesgourgues, The H0 Olympics: A fair ranking of proposed models, *Phys. Rept.* **984**, 1 (2022), [arXiv:2107.10291 \[astro-ph.CO\]](#).
  - [6] P. Shah, P. Lemos, and O. Lahav, A buyer’s guide to the Hubble constant, *Astron. Astrophys. Rev.* **29**, 9 (2021), [arXiv:2109.01161 \[astro-ph.CO\]](#).
  - [7] E. Abdalla *et al.*, Cosmology intertwined: A review of the particle physics, astrophysics, and cosmology associated with the cosmological tensions and anomalies, *JHEAp* **34**, 49 (2022), [arXiv:2203.06142 \[astro-ph.CO\]](#).
  - [8] E. Di Valentino, Challenges of the Standard Cosmological Model, *Universe* **8**, 399 (2022).
  - [9] M. Kamionkowski and A. G. Riess, The Hubble Tension and Early Dark Energy, *Ann. Rev. Nucl. Part. Sci.* **73**, 153 (2023), [arXiv:2211.04492 \[astro-ph.CO\]](#).
  - [10] J.-P. Hu and F.-Y. Wang, Hubble Tension: The Evidence of New Physics, *Universe* **9**, 94 (2023), [arXiv:2302.05709 \[astro-ph.CO\]](#).
  - [11] W. Giarè, CMB Anomalies and the Hubble Tension (2023), [arXiv:2305.16919 \[astro-ph.CO\]](#).
  - [12] L. Verde, N. Schöneberg, and H. Gil-Marín, A tale of many  $H_0$  (2023), [arXiv:2311.13305 \[astro-ph.CO\]](#).
  - [13] E. Di Valentino and D. Brout, eds., *The Hubble Constant Tension*, Springer Series in Astrophysics and Cosmology (Springer, 2024).
  - [14] L. Perivolaropoulos, Hubble Tension or Distance Ladder Crisis? (2024), [arXiv:2408.11031 \[astro-ph.CO\]](#).
  - [15] O. Akarsu, E. O. Colgáin, A. A. Sen, and M. M. Sheikh-Jabbari,  $\Lambda$ CDM Tensions: Localising Missing Physics through Consistency Checks, *Universe* **10**, 305 (2024), [arXiv:2402.04767 \[astro-ph.CO\]](#).
  - [16] T. M. C. Abbott *et al.* (DES), Dark Energy Survey Year 3 results: Cosmological constraints from galaxy clustering and weak lensing, *Phys. Rev. D* **105**, 023520 (2022), [arXiv:2105.13549 \[astro-ph.CO\]](#).
  - [17] M. Asgari *et al.* (KiDS), KiDS-1000 Cosmology: Cosmic shear constraints and comparison between two point statistics, *Astron. Astrophys.* **645**, A104 (2021), [arXiv:2007.15633 \[astro-ph.CO\]](#).
  - [18] C. Heymans *et al.*, KiDS-1000 Cosmology: Multi-probe weak gravitational lensing and spectroscopic galaxy clustering constraints, *Astron. Astrophys.* **646**, A140 (2021), [arXiv:2007.15632 \[astro-ph.CO\]](#).



- [19] T. M. C. Abbott *et al.* (Kilo-Degree Survey, DES), DES Y3 + KiDS-1000: Consistent cosmology combining cosmic shear surveys, *Open J. Astrophys.* **6**, 2305.17173 (2023), [arXiv:2305.17173 \[astro-ph.CO\]](#).
- [20] R. Dalal *et al.*, Hyper Suprime-Cam Year 3 results: Cosmology from cosmic shear power spectra, *Phys. Rev. D* **108**, 123519 (2023), [arXiv:2304.00701 \[astro-ph.CO\]](#).
- [21] S. Chen *et al.*, Analysis of DESI×DES using the Lagrangian effective theory of LSS, *Phys. Rev. D* **110**, 103518 (2024), [arXiv:2407.04795 \[astro-ph.CO\]](#).
- [22] J. Kim *et al.*, The Atacama Cosmology Telescope DR6 and DESI: structure formation over cosmic time with a measurement of the cross-correlation of CMB lensing and luminous red galaxies, *JCAP* **12**, 022, [arXiv:2407.04606 \[astro-ph.CO\]](#).
- [23] L. Faga *et al.* (DES), Dark energy survey year 3 results: cosmology from galaxy clustering and galaxy–galaxy lensing in harmonic space, *Mon. Not. Roy. Astron. Soc.* **536**, 1586 (2024), [arXiv:2406.12675 \[astro-ph.CO\]](#).
- [24] J. Harnois-Deraps *et al.*, KiDS-1000 and DES-Y1 combined: cosmology from peak count statistics, *Mon. Not. Roy. Astron. Soc.* **534**, 3305 (2024), [arXiv:2405.10312 \[astro-ph.CO\]](#).
- [25] F. J. Qu *et al.*, The Atacama Cosmology Telescope DR6 and DESI: Structure growth measurements from the cross-correlation of DESI Legacy Imaging galaxies and CMB lensing from ACT DR6 and Planck PR4 (2024), [arXiv:2410.10808 \[astro-ph.CO\]](#).
- [26] E. Di Valentino and S. Bridle, Exploring the Tension between Current Cosmic Microwave Background and Cosmic Shear Data, *Symmetry* **10**, 585 (2018).
- [27] T. Tröster *et al.*, Cosmology from large-scale structure: Constraining  $\Lambda$ CDM with BOSS, *Astron. Astrophys.* **633**, L10 (2020), [arXiv:1909.11006 \[astro-ph.CO\]](#).
- [28] E. Di Valentino *et al.*, Cosmology Intertwined III:  $f\sigma_8$  and  $S_8$ , *Astropart. Phys.* **131**, 102604 (2021), [arXiv:2008.11285 \[astro-ph.CO\]](#).
- [29] S. A. Adil, O. Akarsu, M. Malekjani, E. O. Colgáin, S. Pourojaghi, A. A. Sen, and M. M. Sheikh-Jabbari,  $S_8$  increases with effective redshift in  $\Lambda$ CDM cosmology, *Mon. Not. Roy. Astron. Soc.* **528**, L20 (2023), [arXiv:2303.06928 \[astro-ph.CO\]](#).
- [30] O. Akarsu, E. O. Colgáin, A. A. Sen, and M. M. Sheikh-Jabbari, Further support for  $S_8$  increasing with effective redshift (2024), [arXiv:2410.23134 \[astro-ph.CO\]](#).
- [31] N.-M. Nguyen, D. Huterer, and Y. Wen, Evidence for Suppression of Structure Growth in the Concordance Cosmological Model, *Phys. Rev. Lett.* **131**, 111001 (2023), [arXiv:2302.01331 \[astro-ph.CO\]](#).
- [32] E. Specogna, E. Di Valentino, J. Levi Said, and N.-M. Nguyen, Exploring the growth index  $\gamma_L$ : Insights from different CMB dataset combinations and approaches, *Phys. Rev. D* **109**, 043528 (2024), [arXiv:2305.16865 \[astro-ph.CO\]](#).
- [33] L.-M. Wang and P. J. Steinhardt, Cluster abundance constraints on quintessence models, *Astrophys. J.* **508**, 483 (1998), [arXiv:astro-ph/9804015](#).
- [34] E. V. Linder, Cosmic growth history and expansion history, *Phys. Rev. D* **72**, 043529 (2005), [arXiv:astro-ph/0507263](#).
- [35] D. Huterer, Growth of cosmic structure, *Astron. Astrophys. Rev.* **31**, 2 (2023), [arXiv:2212.05003 \[astro-ph.CO\]](#).
- [36] N. Aghanim *et al.* (Planck), Planck 2018 results. VI. Cosmological parameters, *Astron. Astrophys.* **641**, A6 (2020), [Erratum: *Astron. Astrophys.* 652, C4 (2021)], [arXiv:1807.06209 \[astro-ph.CO\]](#).
- [37] E. Calabrese, A. Slosar, A. Melchiorri, G. F. Smoot, and O. Zahn, Cosmic Microwave Weak lensing data as a test for the dark universe, *Phys. Rev. D* **77**, 123531 (2008), [arXiv:0803.2309 \[astro-ph\]](#).
- [38] E. Di Valentino, A. Melchiorri, and J. Silk, Investigating Cosmic Discordance, *Astrophys. J. Lett.* **908**, L9 (2021), [arXiv:2003.04935 \[astro-ph.CO\]](#).
- [39] E. Specogna, W. Giarè, and E. Di Valentino, Planck-PR4 anisotropy spectra show (better) consistency with General Relativity (2024), [arXiv:2411.03896 \[astro-ph.CO\]](#).
- [40] O. Akarsu, J. D. Barrow, L. A. Escamilla, and J. A. Vazquez, Graduated dark energy: Observational hints of a spontaneous sign switch in the cosmological constant, *Phys. Rev. D* **101**, 063528 (2020), [arXiv:1912.08751 \[astro-ph.CO\]](#).
- [41] O. Akarsu, S. Kumar, E. Özülker, and J. A. Vazquez, Relaxing cosmological tensions with a sign switching cosmological constant, *Phys. Rev. D* **104**, 123512 (2021), [arXiv:2108.09239 \[astro-ph.CO\]](#).
- [42] O. Akarsu, S. Kumar, E. Özülker, J. A. Vazquez, and A. Yadav, Relaxing cosmological tensions with a sign switching cosmological constant: Improved results with Planck, BAO, and Pantheon data, *Phys. Rev. D* **108**, 023513 (2023), [arXiv:2211.05742 \[astro-ph.CO\]](#).
- [43] O. Akarsu, E. Di Valentino, S. Kumar, R. C. Nunes, J. A. Vazquez, and A. Yadav,  $\Lambda_s$ CDM model: A promising scenario for alleviation of cosmological tensions (2023), [arXiv:2307.10899 \[astro-ph.CO\]](#).
- [44] O. Akarsu, A. De Felice, E. Di Valentino, S. Kumar, R. C. Nunes, E. Ozulker, J. A. Vazquez, and A. Yadav,  $\Lambda_s$ CDM cosmology from a type-II minimally modified gravity (2024), [arXiv:2402.07716 \[astro-ph.CO\]](#).
- [45] O. Akarsu, A. De Felice, E. Di Valentino, S. Kumar, R. C. Nunes, E. Özülker, J. A. Vazquez, and A. Yadav, Cosmological constraints on  $\Lambda_s$ CDM scenario in a type II minimally modified gravity, *Phys. Rev. D* **110**, 103527 (2024), [arXiv:2406.07526 \[astro-ph.CO\]](#).
- [46] A. Yadav, S. Kumar, C. Kibris, and O. Akarsu,  $\Lambda_s$ CDM cosmology: alleviating major cosmological tensions by predicting standard neutrino properties, *JCAP* **01**, 042, [arXiv:2406.18496 \[astro-ph.CO\]](#).
- [47] N. Craig, D. Green, J. Meyers, and S. Rajendran, No  $\nu s$  is Good News, *JHEP* **09**, 097, [arXiv:2405.00836 \[astro-ph.CO\]](#).
- [48] D. Wang, O. Mena, E. Di Valentino, and S. Gariazzo, Updating neutrino mass constraints with background measurements, *Phys. Rev. D* **110**, 103536 (2024), [arXiv:2405.03368 \[astro-ph.CO\]](#).
- [49] D. Green and J. Meyers, The Cosmological Preference for Negative Neutrino Mass (2024), [arXiv:2407.07878 \[astro-ph.CO\]](#).
- [50] L. Herold, E. G. M. Ferreira, and L. Heinrich, Profile Likelihoods in Cosmology: When, Why and How illustrated with  $\Lambda$ CDM, Massive Neutrinos and Dark Energy (2024), [arXiv:2408.07700 \[astro-ph.CO\]](#).
- [51] S.-F. Ge and L. Tan, Capability of Cosmic Gravitational Focusing on Identifying the Neutrino Mass Ordering (2024), [arXiv:2409.11115 \[hep-ph\]](#).
- [52] J.-Q. Jiang, W. Giarè, S. Gariazzo, M. G. Dainotti, E. Di Valentino, O. Mena, D. Pedrotti, S. S. da Costa, and S. Vagnozzi, Neutrino cosmology after DESI: tightest



- mass upper limits, preference for the normal ordering, and tension with terrestrial observations, *JCAP* **01**, 153, [arXiv:2407.18047 \[astro-ph.CO\]](#).
- [53] W. Elbers, C. S. Frenk, A. Jenkins, B. Li, and S. Pascoli, Negative neutrino masses as a mirage of dark energy (2024), [arXiv:2407.10965 \[astro-ph.CO\]](#).
  - [54] J. D. Barrow, Sudden future singularities, *Class. Quant. Grav.* **21**, L79 (2004), [arXiv:gr-qc/0403084](#).
  - [55] E. A. Paraskevas, A. Cam, L. Perivolaropoulos, and O. Akarsu, Transition dynamics in the  $\Lambda$ CDM model: Implications for bound cosmic structures, *Phys. Rev. D* **109**, 103522 (2024), [arXiv:2402.05908 \[astro-ph.CO\]](#).
  - [56] B. Alexandre, S. Gielen, and J. a. Magueijo, Overall signature of the metric and the cosmological constant, *JCAP* **02**, 036, [arXiv:2306.11502 \[hep-th\]](#).
  - [57] L. A. Anchordoqui, I. Antoniadis, and D. Lust, Anti-de Sitter  $\rightarrow$  de Sitter transition driven by Casimir forces and mitigating tensions in cosmological parameters, *Phys. Lett. B* **855**, 138775 (2024), [arXiv:2312.12352 \[hep-th\]](#).
  - [58] L. A. Anchordoqui, I. Antoniadis, D. Lust, N. T. Noble, and J. F. Soriano, From infinite to infinitesimal: Using the universe as a dataset to probe Casimir corrections to the vacuum energy from fields inhabiting the dark dimension, *Phys. Dark Univ.* **46**, 101715 (2024), [arXiv:2404.17334 \[astro-ph.CO\]](#).
  - [59] L. A. Anchordoqui, I. Antoniadis, D. Bielli, A. Chatrabhuti, and H. Isono, Thin-wall vacuum decay in the presence of a compact dimension meets the  $H_0$  and  $S_8$  tensions (2024), [arXiv:2410.18649 \[hep-th\]](#).
  - [60] O. Akarsu, B. Bulduk, A. De Felice, N. Katirci, and N. M. Uzun, Unexplored regions in teleparallel  $f(T)$  gravity: Sign-changing dark energy density (2024), [arXiv:2410.23068 \[gr-qc\]](#).
  - [61] M. S. Souza, A. M. Barcelos, R. C. Nunes, O. Akarsu, and S. Kumar, Mapping the  $\Lambda$ CDM Scenario to  $f(T)$  Modified Gravity: Effects on Structure Growth Rate (2025), [arXiv:2501.18031 \[astro-ph.CO\]](#).
  - [62] O. Akarsu, L. Perivolaropoulos, A. Tsikoundoura, A. E. Yükselci, and A. Zhuk, Dynamical dark energy with AdS-to-dS and dS-to-dS transitions: Implications for the  $H_0$  tension (2025), [arXiv:2502.14667 \[astro-ph.CO\]](#).
  - [63] V. Sahni and Y. Shtanov, Brane world models of dark energy, *JCAP* **11**, 014, [arXiv:astro-ph/0202346](#).
  - [64] J. A. Vazquez, S. Hee, M. P. Hobson, A. N. Lasenby, M. Ibison, and M. Bridges, Observational constraints on conformal time symmetry, missing matter and double dark energy, *JCAP* **07**, 062, [arXiv:1208.2542 \[astro-ph.CO\]](#).
  - [65] T. Delubac *et al.* (BOSS), Baryon acoustic oscillations in the Ly $\alpha$  forest of BOSS DR11 quasars, *Astron. Astrophys.* **574**, A59 (2015), [arXiv:1404.1801 \[astro-ph.CO\]](#).
  - [66] V. Sahni, A. Shafieloo, and A. A. Starobinsky, Model independent evidence for dark energy evolution from Baryon Acoustic Oscillations, *Astrophys. J. Lett.* **793**, L40 (2014), [arXiv:1406.2209 \[astro-ph.CO\]](#).
  - [67] E. Aubourg *et al.* (BOSS), Cosmological implications of baryon acoustic oscillation measurements, *Phys. Rev. D* **92**, 123516 (2015), [arXiv:1411.1074 \[astro-ph.CO\]](#).
  - [68] E. Di Valentino, E. V. Linder, and A. Melchiorri, Vacuum phase transition solves the  $H_0$  tension, *Phys. Rev. D* **97**, 043528 (2018), [arXiv:1710.02153 \[astro-ph.CO\]](#).
  - [69] E. Mörtzell and S. Dhawan, Does the Hubble constant tension call for new physics?, *JCAP* **09**, 025, [arXiv:1801.07260 \[astro-ph.CO\]](#).
  - [70] V. Poulin, K. K. Boddy, S. Bird, and M. Kamionkowski, Implications of an extended dark energy cosmology with massive neutrinos for cosmological tensions, *Phys. Rev. D* **97**, 123504 (2018), [arXiv:1803.02474 \[astro-ph.CO\]](#).
  - [71] S. Capozziello, Ruchika, and A. A. Sen, Model independent constraints on dark energy evolution from low-redshift observations, *Mon. Not. Roy. Astron. Soc.* **484**, 4484 (2019), [arXiv:1806.03943 \[astro-ph.CO\]](#).
  - [72] Y. Wang, L. Pogosian, G.-B. Zhao, and A. Zucca, Evolution of dark energy reconstructed from the latest observations, *Astrophys. J. Lett.* **869**, L8 (2018), [arXiv:1807.03772 \[astro-ph.CO\]](#).
  - [73] A. Banihashemi, N. Khosravi, and A. H. Shirazi, Phase transition in the dark sector as a proposal to lessen cosmological tensions, *Phys. Rev. D* **101**, 123521 (2020), [arXiv:1808.02472 \[astro-ph.CO\]](#).
  - [74] K. Dutta, Ruchika, A. Roy, A. A. Sen, and M. M. Sheikh-Jabbari, Beyond  $\Lambda$ CDM with low and high redshift data: implications for dark energy, *Gen. Rel. Grav.* **52**, 15 (2020), [arXiv:1808.06623 \[astro-ph.CO\]](#).
  - [75] A. Banihashemi, N. Khosravi, and A. H. Shirazi, Ginzburg-Landau Theory of Dark Energy: A Framework to Study Both Temporal and Spatial Cosmological Tensions Simultaneously, *Phys. Rev. D* **99**, 083509 (2019), [arXiv:1810.11007 \[astro-ph.CO\]](#).
  - [76] O. Akarsu, J. D. Barrow, C. V. R. Board, N. M. Uzun, and J. A. Vazquez, Screening  $\Lambda$  in a new modified gravity model, *Eur. Phys. J. C* **79**, 846 (2019), [arXiv:1903.11519 \[gr-qc\]](#).
  - [77] X. Li and A. Shafieloo, A Simple Phenomenological Emergent Dark Energy Model can Resolve the Hubble Tension, *Astrophys. J. Lett.* **883**, L3 (2019), [arXiv:1906.08275 \[astro-ph.CO\]](#).
  - [78] L. Visinelli, S. Vagnozzi, and U. Danielsson, Revisiting a negative cosmological constant from low-redshift data, *Symmetry* **11**, 1035 (2019), [arXiv:1907.07953 \[astro-ph.CO\]](#).
  - [79] G. Ye and Y.-S. Piao, Is the Hubble tension a hint of AdS phase around recombination?, *Phys. Rev. D* **101**, 083507 (2020), [arXiv:2001.02451 \[astro-ph.CO\]](#).
  - [80] A. Perez, D. Sudarsky, and E. Wilson-Ewing, Resolving the  $H_0$  tension with diffusion, *Gen. Rel. Grav.* **53**, 7 (2021), [arXiv:2001.07536 \[astro-ph.CO\]](#).
  - [81] O. Akarsu, N. Katirci, S. Kumar, R. C. Nunes, B. Öztürk, and S. Sharma, Rastall gravity extension of the standard  $\Lambda$ CDM model: theoretical features and observational constraints, *Eur. Phys. J. C* **80**, 1050 (2020), [arXiv:2004.04074 \[astro-ph.CO\]](#).
  - [82] Ruchika, S. A. Adil, K. Dutta, A. Mukherjee, and A. A. Sen, Observational constraints on axion(s) dark energy with a cosmological constant, *Phys. Dark Univ.* **40**, 101199 (2023), [arXiv:2005.08813 \[astro-ph.CO\]](#).
  - [83] E. Di Valentino, A. Mukherjee, and A. A. Sen, Dark Energy with Phantom Crossing and the  $H_0$  Tension, *Entropy* **23**, 404 (2021), [arXiv:2005.12587 \[astro-ph.CO\]](#).
  - [84] R. Calderón, R. Gannouji, B. L'Huillier, and D. Polarski, Negative cosmological constant in the dark sector?, *Phys. Rev. D* **103**, 023526 (2021), [arXiv:2008.10237 \[astro-ph.CO\]](#).
  - [85] G. Ye and Y.-S. Piao,  $T_0$  censorship of early dark energy and AdS vacua, *Phys. Rev. D* **102**, 083523 (2020), [arXiv:2008.10832 \[astro-ph.CO\]](#).

- [86] A. De Felice, S. Mukohyama, and M. C. Pookkillath, Addressing  $H_0$  tension by means of  $\Lambda$ CDM, *Phys. Lett. B* **816**, 136201 (2021), [Erratum: *Phys. Lett. B* 818, 136364 (2021)], [arXiv:2009.08718 \[astro-ph.CO\]](#).
- [87] A. Paliathanasis and G. Leon, Dynamics of a two scalar field cosmological model with phantom terms, *Class. Quant. Grav.* **38**, 075013 (2021), [arXiv:2009.12874 \[gr-qc\]](#).
- [88] A. Bonilla, S. Kumar, and R. C. Nunes, Measurements of  $H_0$  and reconstruction of the dark energy properties from a model-independent joint analysis, *Eur. Phys. J. C* **81**, 127 (2021), [arXiv:2011.07140 \[astro-ph.CO\]](#).
- [89] G. Acquaviva, O. Akarsu, N. Katirci, and J. A. Vazquez, Simple-graduated dark energy and spatial curvature, *Phys. Rev. D* **104**, 023505 (2021), [arXiv:2104.02623 \[astro-ph.CO\]](#).
- [90] S. Bag, V. Sahni, A. Shafieloo, and Y. Shtanov, Phantom Braneworld and the Hubble Tension, *Astrophys. J.* **923**, 212 (2021), [arXiv:2107.03271 \[astro-ph.CO\]](#).
- [91] R. C. Bernardo, D. Grandón, J. Said Levi, and V. H. Cárdenas, Parametric and nonparametric methods hint dark energy evolution, *Phys. Dark Univ.* **36**, 101017 (2022), [arXiv:2111.08289 \[astro-ph.CO\]](#).
- [92] L. A. Escamilla and J. A. Vazquez, Model selection applied to reconstructions of the Dark Energy, *Eur. Phys. J. C* **83**, 251 (2023), [arXiv:2111.10457 \[astro-ph.CO\]](#).
- [93] A. A. Sen, S. A. Adil, and S. Sen, Do cosmological observations allow a negative  $\Lambda$ ?, *Mon. Not. Roy. Astron. Soc.* **518**, 1098 (2022), [arXiv:2112.10641 \[astro-ph.CO\]](#).
- [94] E. Ozulker, Is the dark energy equation of state parameter singular?, *Phys. Rev. D* **106**, 063509 (2022), [arXiv:2203.04167 \[astro-ph.CO\]](#).
- [95] S. Di Gennaro and Y. C. Ong, Sign Switching Dark Energy from a Running Barrow Entropy, *Universe* **8**, 541 (2022), [arXiv:2205.09311 \[gr-qc\]](#).
- [96] O. Akarsu, E. O. Colgain, E. Özülker, S. Thakur, and L. Yin, Inevitable manifestation of wiggles in the expansion of the late Universe, *Phys. Rev. D* **107**, 123526 (2023), [arXiv:2207.10609 \[astro-ph.CO\]](#).
- [97] H. Moshafi, H. Firouzjahi, and A. Talebian, Multiple Transitions in Vacuum Dark Energy and  $H_0$  Tension, *Astrophys. J.* **940**, 121 (2022), [arXiv:2208.05583 \[astro-ph.CO\]](#).
- [98] R. C. Bernardo, D. Grandón, J. Levi Said, and V. H. Cárdenas, Dark energy by natural evolution: Constraining dark energy using Approximate Bayesian Computation, *Phys. Dark Univ.* **40**, 101213 (2023), [arXiv:2211.05482 \[astro-ph.CO\]](#).
- [99] A. van de Venn, D. Vasak, J. Kirsch, and J. Struckmeier, Torsional dark energy in quadratic gauge gravity, *Eur. Phys. J. C* **83**, 288 (2023), [arXiv:2211.11868 \[gr-qc\]](#).
- [100] Y. C. Ong, An Effective Sign Switching Dark Energy: Lotka–Volterra Model of Two Interacting Fluids, *Universe* **9**, 437 (2023), [arXiv:2212.04429 \[gr-qc\]](#).
- [101] Y. Tiwari, B. Ghosh, and R. K. Jain, Towards a possible solution to the Hubble tension with Horndeski gravity, *Eur. Phys. J. C* **84**, 220 (2024), [arXiv:2301.09382 \[astro-ph.CO\]](#).
- [102] M. Malekjani, R. M. Conville, E. O. Colgáin, S. Pourojaghi, and M. M. Sheikh-Jabbari, On redshift evolution and negative dark energy density in Pantheon + Supernovae, *Eur. Phys. J. C* **84**, 317 (2024), [arXiv:2301.12725 \[astro-ph.CO\]](#).
- [103] J. A. Vázquez, D. Tamayo, G. Garcia-Arroyo, I. Gómez-Vargas, I. Quiros, and A. A. Sen, Coupled multiscalar field dark energy, *Phys. Rev. D* **109**, 023511 (2024), [arXiv:2305.11396 \[astro-ph.CO\]](#).
- [104] L. A. Escamilla, O. Akarsu, E. Di Valentino, and J. A. Vazquez, Model-independent reconstruction of the interacting dark energy kernel: Binned and Gaussian process, *JCAP* **11**, 051, [arXiv:2305.16290 \[astro-ph.CO\]](#).
- [105] S. A. Adil, O. Akarsu, E. Di Valentino, R. C. Nunes, E. Özülker, A. A. Sen, and E. Specogna, Omnipotent dark energy: A phenomenological answer to the Hubble tension, *Phys. Rev. D* **109**, 023527 (2024), [arXiv:2306.08046 \[astro-ph.CO\]](#).
- [106] S. A. Adil, U. Mukhopadhyay, A. A. Sen, and S. Vagnozzi, Dark energy in light of the early JWST observations: case for a negative cosmological constant?, *JCAP* **10**, 072, [arXiv:2307.12763 \[astro-ph.CO\]](#).
- [107] E. A. Paraskevas and L. Perivolaropoulos, The density of virialized clusters as a probe of dark energy, *Mon. Not. Roy. Astron. Soc.* **531**, 1021 (2024), [arXiv:2308.07046 \[astro-ph.CO\]](#).
- [108] A. Gómez-Valent, A. Favale, M. Migliaccio, and A. A. Sen, Late-time phenomenology required to solve the  $H_0$  tension in view of the cosmic ladders and the anisotropic and angular BAO datasets, *Phys. Rev. D* **109**, 023525 (2024), [arXiv:2309.07795 \[astro-ph.CO\]](#).
- [109] R. Y. Wen, L. T. Hergt, N. Afshordi, and D. Scott, A cosmic glitch in gravity, *JCAP* **03**, 045, [arXiv:2311.03028 \[astro-ph.CO\]](#).
- [110] R. Medel-Esquivel, I. Gómez-Vargas, A. A. M. Sánchez, R. García-Salcedo, and J. Alberto Vázquez, Cosmological Parameter Estimation with Genetic Algorithms, *Universe* **10**, 11 (2024), [arXiv:2311.05699 \[astro-ph.CO\]](#).
- [111] A. De Felice, S. Kumar, S. Mukohyama, and R. C. Nunes, Observational bounds on extended minimal theories of massive gravity: new limits on the graviton mass, *JCAP* **04**, 013, [arXiv:2311.10530 \[astro-ph.CO\]](#).
- [112] N. Menci, S. A. Adil, U. Mukhopadhyay, A. A. Sen, and S. Vagnozzi, Negative cosmological constant in the dark energy sector: tests from JWST photometric and spectroscopic observations of high-redshift galaxies, *JCAP* **07**, 072, [arXiv:2401.12659 \[astro-ph.CO\]](#).
- [113] A. Gomez-Valent and J. Solà Peracaula, Phantom Matter: A Challenging Solution to the Cosmological Tensions, *Astrophys. J.* **975**, 64 (2024), [arXiv:2404.18845 \[astro-ph.CO\]](#).
- [114] R. Calderon *et al.* (DESI), DESI 2024: reconstructing dark energy using crossing statistics with DESI DR1 BAO data, *JCAP* **10**, 048, [arXiv:2405.04216 \[astro-ph.CO\]](#).
- [115] D. Bousis and L. Perivolaropoulos, Hubble tension tomography: BAO vs SN Ia distance tension, *Phys. Rev. D* **110**, 103546 (2024), [arXiv:2405.07039 \[astro-ph.CO\]](#).
- [116] H. Wang, Z.-Y. Peng, and Y.-S. Piao, Can recent DESI BAO measurements accommodate a negative cosmological constant? (2024), [arXiv:2406.03395 \[astro-ph.CO\]](#).
- [117] E. O. Colgáin, S. Pourojaghi, and M. M. Sheikh-Jabbari, Implications of DES 5YR SNe Dataset for  $\Lambda$ CDM (2024), [arXiv:2406.06389 \[astro-ph.CO\]](#).
- [118] U. K. Tyagi, S. Haridasu, and S. Basak, Holographic and gravity-thermodynamic approaches in entropic cosmology: Bayesian assessment using late-time data, *Phys. Rev. D* **110**, 063503 (2024), [arXiv:2406.07446 \[astro-ph.CO\]](#).

- ph.CO].
- [119] Y. Toda, W. Giarè, E. Özülker, E. Di Valentino, and S. Vagnozzi, Combining pre- and post-recombination new physics to address cosmological tensions: Case study with varying electron mass and sign-switching cosmological constant, *Phys. Dark Univ.* **46**, 101676 (2024), [arXiv:2407.01173 \[astro-ph.CO\]](#).
  - [120] M. A. Sabogal, O. Akarsu, A. Bonilla, E. Di Valentino, and R. C. Nunes, Exploring new physics in the late Universe's expansion through non-parametric inference, *Eur. Phys. J. C* **84**, 703 (2024), [arXiv:2407.04223 \[astro-ph.CO\]](#).
  - [121] S. Dwivedi and M. Högsås, 2D BAO vs. 3D BAO: Solving the Hubble Tension with Bimetric Cosmology, *Universe* **10**, 406 (2024), [arXiv:2407.04322 \[astro-ph.CO\]](#).
  - [122] L. A. Escamilla, E. Özülker, O. Akarsu, E. Di Valentino, and J. A. Vázquez, Do we need wavelets in the late Universe? (2024), [arXiv:2408.12516 \[astro-ph.CO\]](#).
  - [123] A. Gómez-Valent and J. Solà Peracaula, Composite Dark Energy and the Cosmological Tensions (2024), [arXiv:2412.15124 \[astro-ph.CO\]](#).
  - [124] M. T. Manoharan, Insights on Granda–Oliveros holographic dark energy: possibility of negative dark energy at  $z \gtrsim 2$ , *Eur. Phys. J. C* **84**, 552 (2024).
  - [125] P. Mukherjee, D. Kumar, and A. A. Sen, Quintessential Implications of the presence of AdS in the Dark Energy sector (2025), [arXiv:2501.18335 \[astro-ph.CO\]](#).
  - [126] W. Giarè, T. Mahassen, E. Di Valentino, and S. Pan, An overview of what current data can (and cannot yet) say about evolving dark energy (2025), [arXiv:2502.10264 \[astro-ph.CO\]](#).
  - [127] R. E. Keeley, K. N. Abazajian, M. Kaplinghat, and A. Shafieloo, The Preference for Evolving Dark Energy from Cosmological Distance Measurements and Possible Signatures in the Growth Rate of Perturbations (2025), [arXiv:2502.12667 \[astro-ph.CO\]](#).
  - [128] J. F. Soriano, S. Wohlberg, and L. A. Anchordoqui, New insights on a sign-switching  $\Lambda$  (2025), [arXiv:2502.19239 \[astro-ph.CO\]](#).
  - [129] D. Efstratiou and L. Perivolaropoulos, Metastable Cosmological Constant and Gravitational Bubbles: Ultra-Late-Time Transitions in Modified Gravity (2025), [arXiv:2503.11365 \[gr-qc\]](#).
  - [130] S. Kumar and R. C. Nunes, Echo of interactions in the dark sector, *Phys. Rev. D* **96**, 103511 (2017), [arXiv:1702.02143 \[astro-ph.CO\]](#).
  - [131] E. Di Valentino, A. Melchiorri, and O. Mena, Can interacting dark energy solve the  $H_0$  tension?, *Phys. Rev. D* **96**, 043503 (2017), [arXiv:1704.08342 \[astro-ph.CO\]](#).
  - [132] W. Yang, A. Mukherjee, E. Di Valentino, and S. Pan, Interacting dark energy with time varying equation of state and the  $H_0$  tension, *Phys. Rev. D* **98**, 123527 (2018), [arXiv:1809.06883 \[astro-ph.CO\]](#).
  - [133] S. Kumar, R. C. Nunes, and S. K. Yadav, Dark sector interaction: a remedy of the tensions between CMB and LSS data, *Eur. Phys. J. C* **79**, 576 (2019), [arXiv:1903.04865 \[astro-ph.CO\]](#).
  - [134] S. Pan, W. Yang, E. Di Valentino, E. N. Saridakis, and S. Chakraborty, Interacting scenarios with dynamical dark energy: Observational constraints and alleviation of the  $H_0$  tension, *Phys. Rev. D* **100**, 103520 (2019), [arXiv:1907.07540 \[astro-ph.CO\]](#).
  - [135] E. Di Valentino, A. Melchiorri, O. Mena, and S. Vagnozzi, Interacting dark energy in the early 2020s: A promising solution to the  $H_0$  and cosmic shear tensions, *Phys. Dark Univ.* **30**, 100666 (2020), [arXiv:1908.04281 \[astro-ph.CO\]](#).
  - [136] E. Di Valentino, A. Melchiorri, O. Mena, and S. Vagnozzi, Nonminimal dark sector physics and cosmological tensions, *Phys. Rev. D* **101**, 063502 (2020), [arXiv:1910.09853 \[astro-ph.CO\]](#).
  - [137] M. Lucca and D. C. Hooper, Shedding light on dark matter-dark energy interactions, *Phys. Rev. D* **102**, 123502 (2020), [arXiv:2002.06127 \[astro-ph.CO\]](#).
  - [138] A. Gómez-Valent, V. Pettorino, and L. Amendola, Update on coupled dark energy and the  $H_0$  tension, *Phys. Rev. D* **101**, 123513 (2020), [arXiv:2004.00610 \[astro-ph.CO\]](#).
  - [139] S. Kumar, Remedy of some cosmological tensions via effective phantom-like behavior of interacting vacuum energy, *Phys. Dark Univ.* **33**, 100862 (2021), [arXiv:2102.12902 \[astro-ph.CO\]](#).
  - [140] R. C. Nunes, S. Vagnozzi, S. Kumar, E. Di Valentino, and O. Mena, New tests of dark sector interactions from the full-shape galaxy power spectrum, *Phys. Rev. D* **105**, 123506 (2022), [arXiv:2203.08093 \[astro-ph.CO\]](#).
  - [141] A. Bernui, E. Di Valentino, W. Giarè, S. Kumar, and R. C. Nunes, Exploring the  $H_0$  tension and the evidence for dark sector interactions from 2D BAO measurements, *Phys. Rev. D* **107**, 103531 (2023), [arXiv:2301.06097 \[astro-ph.CO\]](#).
  - [142] W. Giarè, M. A. Sabogal, R. C. Nunes, and E. Di Valentino, Interacting Dark Energy after DESI Baryon Acoustic Oscillation Measurements, *Phys. Rev. Lett.* **133**, 251003 (2024), [arXiv:2404.15232 \[astro-ph.CO\]](#).
  - [143] W. Giarè, M. Najafi, S. Pan, E. Di Valentino, and J. T. Firouzjaee, Robust preference for Dynamical Dark Energy in DESI BAO and SN measurements, *JCAP* **10**, 035, [arXiv:2407.16689 \[astro-ph.CO\]](#).
  - [144] W. Giarè, Dynamical Dark Energy Beyond Planck? Constraints from multiple CMB probes, DESI BAO and Type-Ia Supernovae (2024), [arXiv:2409.17074 \[astro-ph.CO\]](#).
  - [145] M. A. Sabogal, E. Silva, R. C. Nunes, S. Kumar, and E. Di Valentino, Sign switching in dark sector coupling interactions as a candidate for resolving cosmological tensions, *Phys. Rev. D* **111**, 043531 (2025), [arXiv:2501.10323 \[astro-ph.CO\]](#).
  - [146] A. G. Adame *et al.* (DESI), DESI 2024 VI: Cosmological Constraints from the Measurements of Baryon Acoustic Oscillations, (2024), [arXiv:2404.03002 \[astro-ph.CO\]](#).
  - [147] O. Akarsu, A. Çam, E. A. Paraskevas, and L. Perivolaropoulos, Linear matter density perturbations in the  $\Lambda_s$ CDM model: Examining growth dynamics and addressing the  $S_8$  tension (2025), [arXiv:2502.20384 \[astro-ph.CO\]](#).
  - [148] J. Torrado and A. Lewis, Cobaya: Code for Bayesian Analysis of hierarchical physical models, *JCAP* **05**, 057, [arXiv:2005.05290 \[astro-ph.IM\]](#).
  - [149] A. Lewis, A. Challinor, and A. Lasenby, Efficient computation of CMB anisotropies in closed FRW models, *Astrophys. J.* **538**, 473 (2000), [arXiv:astro-ph/9911177](#).
  - [150] [https://github.com/MinhMPA/CAMB\\_GammaPrime\\_Growth](https://github.com/MinhMPA/CAMB_GammaPrime_Growth).

- [151] A. Gelman and D. B. Rubin, Inference from Iterative Simulation Using Multiple Sequences, *Statist. Sci.* **7**, 457 (1992).
- [152] N. Aghanim *et al.* (Planck), Planck 2018 results. I. Overview and the cosmological legacy of Planck, *Astron. Astrophys.* **641**, A1 (2020), [arXiv:1807.06205 \[astro-ph.CO\]](#).
- [153] K. Said, M. Colless, C. Magoulas, J. R. Lucey, and M. J. Hudson, Joint analysis of 6dFGS and SDSS peculiar velocities for the growth rate of cosmic structure and tests of gravity, *Mon. Not. Roy. Astron. Soc.* **497**, 1275 (2020), [arXiv:2007.04993 \[astro-ph.CO\]](#).
- [154] F. Beutler, C. Blake, M. Colless, D. H. Jones, L. Staveley-Smith, G. B. Poole, L. Campbell, Q. Parker, W. Saunders, and F. Watson, The 6dF Galaxy Survey:  $z \approx 0$  measurements of the growth rate and  $\sigma_8$ , *Mon. Not. Roy. Astron. Soc.* **423**, 3430 (2012), [arXiv:1204.4725 \[astro-ph.CO\]](#).
- [155] D. Huterer, D. Shafer, D. Scolnic, and F. Schmidt, Testing  $\Lambda$ CDM at the lowest redshifts with SN Ia and galaxy velocities, *JCAP* **05**, 015, [arXiv:1611.09862 \[astro-ph.CO\]](#).
- [156] S. S. Boruah, M. J. Hudson, and G. Lavaux, Cosmic flows in the nearby Universe: new peculiar velocities from SNe and cosmological constraints, *Mon. Not. Roy. Astron. Soc.* **498**, 2703 (2020), [arXiv:1912.09383 \[astro-ph.CO\]](#).
- [157] R. J. Turner, C. Blake, and R. Ruggeri, A local measurement of the growth rate from peculiar velocities and galaxy clustering correlations in the 6dF Galaxy Survey, *Mon. Not. Roy. Astron. Soc.* **518**, 2436 (2022), [arXiv:2207.03707 \[astro-ph.CO\]](#).
- [158] C. Blake, S. Brough, M. Colless, C. Contreras, W. Couch, S. Croom, T. Davis, M. J. Drinkwater, K. Forster, D. Gilbank, M. Gladders, K. Glazebrook, B. Jelliffe, R. J. Jurek, I.-H. Li, B. Madore, D. C. Martin, K. Pimbblet, G. B. Poole, M. Pracy, R. Sharp, E. Wisnioski, D. Woods, T. K. Wyder, and H. K. C. Yee, The WiggleZ Dark Energy Survey: the growth rate of cosmic structure since redshift  $z=0.9$ , *Mon. Not. Roy. Astron. Soc.* **415**, 2876 (2011), [arXiv:1104.2948 \[astro-ph.CO\]](#).
- [159] C. Blake *et al.*, Galaxy And Mass Assembly (GAMA): improved cosmic growth measurements using multiple tracers of large-scale structure, *Mon. Not. Roy. Astron. Soc.* **436**, 3089 (2013), [arXiv:1309.5556 \[astro-ph.CO\]](#).
- [160] C. Howlett, A. Ross, L. Samushia, W. Percival, and M. Manera, The clustering of the SDSS main galaxy sample – II. Mock galaxy catalogues and a measurement of the growth of structure from redshift space distortions at  $z = 0.15$ , *Mon. Not. Roy. Astron. Soc.* **449**, 848 (2015), [arXiv:1409.3238 \[astro-ph.CO\]](#).
- [161] T. Okumura *et al.*, The Subaru FMOS galaxy redshift survey (FastSound). IV. New constraint on gravity theory from redshift space distortions at  $z \sim 1.4$ , *Publ. Astron. Soc. Jap.* **68**, 38 (2016), [arXiv:1511.08083 \[astro-ph.CO\]](#).
- [162] A. Pezzotta *et al.*, The VIMOS Public Extragalactic Redshift Survey (VIPERS): The growth of structure at  $0.5 < z < 1.2$  from redshift-space distortions in the clustering of the PDR-2 final sample, *Astron. Astrophys.* **604**, A33 (2017), [arXiv:1612.05645 \[astro-ph.CO\]](#).
- [163] S. Alam *et al.* (eBOSS), Completed SDSS-IV extended Baryon Oscillation Spectroscopic Survey: Cosmological implications from two decades of spectroscopic surveys at the Apache Point Observatory, *Phys. Rev. D* **103**, 083533 (2021), [arXiv:2007.08991 \[astro-ph.CO\]](#).
- [164] D. Scolnic *et al.*, The Pantheon+ Analysis: The Full Data Set and Light-curve Release, *Astrophys. J.* **938**, 113 (2022), [arXiv:2112.03863 \[astro-ph.CO\]](#).
- [165] A. G. Riess *et al.*, A Comprehensive Measurement of the Local Value of the Hubble Constant with 1 km/s/Mpc Uncertainty from the Hubble Space Telescope and the SH0ES Team, *Astrophys. J. Lett.* **934**, L7 (2022), [arXiv:2112.04510 \[astro-ph.CO\]](#).